

Accelerated Article Preview

Omicron escapes the majority of existing SARS-CoV-2 neutralizing antibodies

Received: 7 December 2021

Accepted: 23 December 2021

Accelerated Article Preview Published
online 23 December 2021

Cite this article as: Cao, Y. et al. Omicron escapes the majority of existing SARS-CoV-2 neutralizing antibodies. *Nature* <https://doi.org/10.1038/s41586-021-04385-3> (2021).

Yunlong Cao, Jing Wang, Fanchong Jian, Tianhe Xiao, Weiliang Song, Ayijiang Yisimayi, Weijin Huang, Qianqian Li, Peng Wang, Ran An, Jing Wang, Yao Wang, Xiao Niu, Sijie Yang, Hui Liang, Haiyan Sun, Tao Li, Yuanling Yu, Qianqian Cui, Shuo Liu, Xiaodong Yang, Shuo Du, Zhiying Zhang, Xiaohua Hao, Fei Shao, Ronghua Jin, Xiangxi Wang, Junyu Xiao, Youchun Wang & Xiaoliang Sunney Xie

This is a PDF file of a peer-reviewed paper that has been accepted for publication. Although unedited, the content has been subjected to preliminary formatting. Nature is providing this early version of the typeset paper as a service to our authors and readers. The text and figures will undergo copyediting and a proof review before the paper is published in its final form. Please note that during the production process errors may be discovered which could affect the content, and all legal disclaimers apply.

Omicron escapes the majority of existing SARS-CoV-2 neutralizing antibodies

<https://doi.org/10.1038/s41586-021-04385-3>

Received: 7 December 2021

Accepted: 23 December 2021

Published online: 23 December 2021

Yunlong Cao^{1,2,11}, Jing Wang^{1,3,11}, Fanchong Jian^{1,4,11}, Tianhe Xiao^{1,5,11}, Weiliang Song^{1,3,11}, Ayijiang Yisimayi^{1,3,11}, Weijin Huang^{6,11}, Qianqian Li⁶, Peng Wang¹, Ran An¹, Jing Wang¹, Yao Wang¹, Xiao Niu^{1,4}, Sijie Yang^{1,7}, Hui Liang¹, Haiyan Sun¹, Tao Li⁶, Yuanling Yu⁶, Qianqian Cui⁶, Shuo Liu⁶, Xiaodong Yang⁸, Shuo Du³, Zhiying Zhang³, Xiaohua Hao⁹, Fei Shao¹, Ronghua Jin⁹, Xiangxi Wang¹⁰, Junyu Xiao^{2,3}, Youchun Wang⁶ & Xiaoliang Sunney Xie^{1,2}

The SARS-CoV-2 B.1.1.529 variant (Omicron) contains 15 mutations on the receptor-binding domain (RBD). How Omicron would evade RBD neutralizing antibodies (NAbs) requires immediate investigation. Here, we used high-throughput yeast display screening^{1,2} to determine the RBD escaping mutation profiles for 247 human anti-RBD NAbs and showed that the NAbs could be unsupervised clustered into six epitope groups (A-F), which is highly concordant with knowledge-based structural classifications^{3–5}. Strikingly, various single mutations of Omicron could impair NAbs of different epitope groups. Specifically, NAbs in Group A-D, whose epitope overlap with ACE2-binding motif, are largely escaped by K417N, G446S, E484A, and Q493R. Group E (S309 site)⁶ and F (CR3022 site)⁷ NAbs, which often exhibit broad sarbecovirus neutralizing activity, are less affected by Omicron, but still, a subset of NAbs are escaped by G339D, N440K, and S371L. Furthermore, Omicron pseudovirus neutralization showed that single mutation tolerating NAbs could also be escaped due to multiple synergetic mutations on their epitopes. In total, over 85% of the tested NAbs are escaped by Omicron. Regarding Nab drugs, the neutralization potency of LY-CoV016/LY-CoV555, REGN10933/REGN10987, AZD1061/AZD8895, and BRII-196 were greatly reduced by Omicron, while VIR-7831 and DXP-604 still function at reduced efficacy. Together, data suggest Omicron would cause significant humoral immune evasion, while NAbs targeting the sarbecovirus conserved region remain most effective. Our results offer instructions for developing Nab drugs and vaccines against Omicron and future variants.

The severe acute respiratory syndrome coronavirus 2 (SARS-CoV-2) variant B.1.1.529 was first reported to the World Health Organization (WHO) on 24 November 2021. It appears to be rapidly spreading, and the WHO classified it as a variant of concern (VOC) only two days after, designating it as Omicron^{8,9}. An unusually large number of mutations are found in Omicron, including over 30 in the spike protein (Extended Data Fig. 1a). The receptor-binding domain, responsible for interacting with the Angiotensin-Converting Enzyme 2 (ACE2) receptor, bears 15 of these mutations, including G339D, S371L, S373P, S375F, K417N, N440K, G446S, S477N, T478K, E484A, Q493R, G496S, Q498R, N501Y, and Y505H. Some of these mutations are very concerning due to their well-understood functional consequences, such as K417N and N501Y, which contribute to immune escape and higher

infectivity^{10–13}. Many other mutations' functional impacts remain to be investigated.

The S protein is the target of essentially all NAbs found in the convalescent sera or elicited by vaccines. Most of the N-terminal domain (NTD) neutralizing antibodies target an antigenic “supersite” in NTD, involving the N3 (residues 141 to 156) and N5 (residues 246 to 260) loops^{14,15}, and are thus very prone to NTD mutations. Omicron carries the Δ143–145 mutation, which would alter the N3 loop and most likely result in immune escape of most anti-NTD NAbs (Extended Data Fig. 1b). Compared to NTD targeting NAbs, RBD targeting NAbs are particularly abundant and potent, and display diverse epitopes. Evaluating how Omicron affects the neutralization capability of anti-RBD NAbs of diverse classes and epitopes is urgently needed.

¹Biomedical Pioneering Innovation Center (BIOPIC), Peking University, Beijing, P.R. China. ²Beijing Advanced Innovation Center for Genomics (ICG), Peking University, Beijing, P.R. China. ³School of Life Sciences, Peking University, Beijing, P.R. China. ⁴College of Chemistry and Molecular Engineering, Peking University, Beijing, P.R. China. ⁵Joint Graduate Program of Peking-Tsinghua-NIBS, Academy for Advanced Interdisciplinary Studies, Peking University, Beijing, China. ⁶Division of HIV/AIDS and Sex-transmitted Virus Vaccines, Institute for Biological Product Control, National Institutes for Food and Drug Control (NIFDC), Beijing, P.R. China. ⁷Tsinghua-Peking Center for Life Sciences, Beijing, P.R. China. ⁸Beijing YouAn Hospital, Capital Medical University, Beijing, P.R. China. ⁹Beijing Ditan Hospital, Capital Medical University, Beijing, P.R. China. ¹⁰CAS Key Laboratory of Infection and Immunity, National Laboratory of Macromolecules, Institute of Biophysics, Chinese Academy of Sciences, Beijing, P.R. China. ¹¹These authors contributed equally: Yunlong Cao, Jing Wang, Fanchong Jian, Tianhe Xiao, Weiliang Song, Ayijiang Yisimayi, Weijin Huang. ✉e-mail: yunlongcao@pku.edu.cn; xiangxi@ibp.ac.cn; junyuxiao@pku.edu.cn; wangyc@nifdc.org.cn; sunneyxie@biopic.pku.edu.cn

RBD-directed SARS-CoV-2 NAb can be assigned into different classes or binding sites based on structural analyses by cryo-EM or high-resolution crystallography;^{3–5} however, structural data only indicates the contacting amino acids, but does not infer the escaping mutations for a specific antibody. Recent advances in deep antigen mutation screening using FACS (fluorescence-activated cell sorting)-based yeast display platform has allowed the quick mapping of all single amino acid mutations in the RBD that affect the binding of SARS-CoV-2 RBD NAb.^{1,16} The method has proven highly effective in predicting NAB drug efficacy toward mutations². However, to study how human humoral immunity may react to highly mutated variants like Omicron requires mutation profiling of a large collection of NABs targeting different regions of RBD, and FACS-based yeast display mutation screening is limited by low experimental throughput. Here we further developed a MACS (magnetic-activated cell sorting)-based screening method which increases the throughput near 100-fold and could obtain comparable data quality like FACS (Fig 1a, Extended Data Fig. 2). Using this method, we quickly characterized the RBD escaping mutation profile for a total of 247 NABs (Supplementary Data 1). Half of the NABs were part of the antibodies identified by us using single-cell VDJ sequencing of antigen-specific memory B cells from SARS-CoV-2 convalescents, SARS-CoV-2 vaccinees, and SARS-CoV-1 convalescents who recently received SARS-CoV-2 vaccines (Supplementary Data 2). The other half of NABs were identified by groups worldwide^{3,5,6,11,17–40} (Supplementary Table 1).

The high-throughput screening capability allowed us to classify these NABs into six Epitope Groups (A–F) using unsupervised clustering without dependence on structural studies, and the grouping is highly concordant with the knowledge-based structural classifications^{3–5} (Fig. 1b, c). In particular, Group A–D NABs largely correspond to the RBS A–D NABs described by Yuan et al.⁴, and overlap with the class 1–2 NABs described by Barnes et al.³, in general. The epitopes of these NABs largely overlap with RBD residues involved in the binding to ACE2. Group A and B NABs, represented by LY-CoV016 and AZD8895, respectively, usually can only bind to the 'up' RBD; whereas most of the Group C and D members, such as LY-CoV555 and REGN-10987, bind to RBDs regardless of their 'up' and 'down' conformations. Group E and F NABs are very similar to the class 3 and 4 NABs described by Barnes et al.³, and target the S309/VIR-7831 site and CR3022 site, which could exhibit pan-sarbecovirus neutralization capacity (Fig 1e). Most of these NABs neutralize SARS-CoV-2 using mechanisms other than directly interfering with ACE2 binding.

Inferred from the escaping mutation profiles, various single mutations of Omicron could impair NABs of different epitope groups (Extended Data Fig. 3). Specifically, NABs in Group A–D, whose epitope overlaps with ACE2-binding motif, are largely escaped by single mutations of K417N, G446S, E484A, and Q493R. Also, a subset of NABs of Group E and F are escaped by single mutations of G339D, N440K, S371L, S375F. However, due to the extensive mutations accumulated on Omicron's RBD, studying NAB's response to Omicron only in the single mutation context is insufficient. Indeed, Omicron pseudovirus neutralization and spike enzyme-linked immunosorbent assay (ELISA) showed that single mutation tolerating NABs could also be escaped by Omicron due to multiple synergetic mutations on their epitopes (Fig 1d, Extended Data Fig. 3). In total, over 85% of the tested human NABs are escaped, suggesting that Omicron could cause significant humoral immune evasion and potential antigenic shifting.

It is crucial to analyze how each group of NABs reacts to Omicron to instruct the development of NAB drugs and vaccines. Group A NABs mainly contains the V/H3-53/V/H3-66 germline gene-encoded antibodies, which are abundantly present in our current collection of SARS-CoV-2 neutralizing antibodies^{17,21,22,26,41–43}, including several antibodies that have obtained emergency use authorization (CB6/LY-CoV016)¹⁹ or are currently being studied in clinical trials (P2C-1F11/BR11-196, BD-604/DXP-604)^{18,44} (Fig. 2a, Extended Data Fig. 4a). Group

A NABs often exhibit less somatic mutations and shorter CDR3 length compared to other groups (Extended Data Fig. 5a, b). The epitopes of these antibodies extensively overlap with the binding site of ACE2 and are often evaded by RBD mutations on K417, D420, F456, A475, L455 sites (Fig 2d, Extended Data Fig. 6a, 7a). Most NABs in Group A were already escaped by B.1.351 (Beta) strain (Extended Data Fig. 5d), specifically by K417N (Extended Data Fig. 8a), due to a critical salt bridge interaction between Lys417 and a negatively charged residue in the antibody (Fig. 2g). The NABs that survived Beta strain, such as BR11-196 and DXP-604, are insensitive to the K417N single site change but could also be heavily affected by the combination of K417N and other RBD mutations located on their epitopes, like S477N, Q493R, G496S, Q498R, N501Y, and Y505H of Omicron, causing lost or reduction of neutralization (Fig 2d; Extended Data Fig. 7a).

The V/H1-58 gene-encoded NABs are enriched in Group B (Extended Data Fig. 4b). These NABs such as AZD8895³⁶, REGN-10933⁴², and BD-836⁴⁵ bind to the left shoulder of RBD, often focusing on the far tip (Fig. 2h). These NABs are very sensitive to the change of F486, N487, and G476 (Fig 2b, Extended Data Fig. 6b). Fortunately, F486 and a few other major targeting sites of these NABs are critically involved in ACE2-binding, and therefore they are generally harder to be escaped. A subset of NABs in Group B, such as AZD8895 and BD-836, could survive Beta (Fig 2e); however, Omicron significantly reduced Group B NABs' binding affinity to RBD, potentially through S477N/T478K/E484A on their epitope (Extended Data Fig. 7b)⁴⁶, resulting in the loss of neutralization.

Group C NABs are frequently encoded by V/H1-2 and V/H1-69 (Extended Data Fig. 4c). The majority of NABs in this group could bind to both "up" and "down" RBDs, resulting in higher neutralization potency compared to other groups (Fig. 2c, Extended Data Fig. 5c). Several highly potent antibodies are found in Group C, including BD-368-2/DXP-593⁴⁴, C002³, and LY-CoV555⁴⁷. They bind to the right shoulder of RBD (Fig. 2i), and are mostly prone to the change of E484 (Extended Data Fig. 6c, 7c), such as the E484K mutation found in Beta (Fig. 2f). The E484A mutation seen in Omicron elicited a similar escaping effect, although the change to Ala is slightly subtler, and could be tolerated by certain antibodies in this group (Extended Data Fig. 8b). All Group C NABs tested are escaped by Omicron.

Group D NABs consist of diverse IGHV gene-encoded antibodies (Extended Data Fig. 4d). Prominent members in this group include REGN-10987⁴² and AZD1061³⁶ (Fig. 3a). They further rotate down from the RBD right shoulder towards the S309 site when compared to Group C NABs (Fig. 3g). As a loop formed by residues 440–449 in RBD is critical for the targeting of this group of NABs, they are sensitive to the changes of N440, K444, G446, and N448 (Extended Data Fig. 6d, 7d). Most NABs of Group D remain active against Beta; however, G446S would substantially affect their neutralization capability against Omicron (Fig. 3d). Also, for those NABs that could tolerate G446S single mutation, the N440K/G446S combination may significantly reduce their binding affinity, resulting in that most Group D NABs are escaped by Omicron.

Group E and F NABs are rarer when compared to the other four groups. The archetypical member of each group was originally isolated from a SARS-CoV-1 convalescent, and displays SARS-CoV-2 cross-neutralizing activity. There is no clear VDJ convergent effect compared to Group A, B, and C (Extended Data Fig. 4e, f), and the mutation rate and CDR3 length are larger than other groups. NABs in Group E and F rarely compete with ACE2; thus, their average half-maximal inhibitory concentration (IC50) is higher than NABs in Group A–D (Extended Data Fig. 5c). NABs in Group E, such as VIR-7831/S309, may recognize a mixed protein/carbohydrate epitope, involving the N-linked glycan on N343⁶ (Fig. 3h). Inferred from the escaping mutation profiles (Fig. 3b), Group E NABs are often sensitive to changes of G339, T345, and R346 (Extended Data Fig. 6e, 7e). The G339D mutation would affect a subset of NABs' neutralization performance (Fig. 3e). Also, part of Group E NABs' epitope would extend to the 440–449 loop, making them sensitive to N440K in Omicron (Fig. 3e). Noticeably, the population of Omicron with R346K is

continuously increasing, which may severely affect the neutralization capacity of Group E NABs.

Group F NABs such as S304 target a cryptic site in RBD that is generally not exposed (Fig. 3i), therefore their neutralizing activities are generally weaker⁷. Group F NABs are often sensitive to changes of F374, T376, and K378 (Extended Data Fig. 6f, 7f). A loop involving RBD residues 371–375 lies in the ridge between the E and F sites; therefore, a subset of Group F NABs, including some Group E NABs, could be affected by the S371L/S373P/S375F mutations if their epitopes extend to this region (Fig. 3c, f). Interestingly, a part of Group F NABs is highly sensitive to V503 and G504, similar to the epitopes of S2X259 (Fig. 3f, j), suggesting that they can compete with ACE2. Indeed, several NABs, such as BD55–5300 and BD55–3372, exhibit higher neutralization potency than other NABs in Group F (Fig. 3c, 4b). However, These antibodies' neutralization capability might be undermined by N501Y and Y505H of Omicron (Fig. 3j).

As for NAB drugs, consistent with their escaping mutation profiles, the neutralization potency of LY-CoV016/LY-CoV555, REGN-10933/REGN-10987, and AZD1061 are greatly reduced by Omicron (Fig. 4a, Extended Data Fig. 9). The binding affinity of AZD8895 and BR11-196 toward Omicron RBD is also significantly reduced, likely due to multiple mutations accumulating on their epitopes, such that AZD8895 and BR11-196 failed to neutralize Omicron (Extended Data Fig. 10). BR11-198 was not tested since the antibody sequence was not released. VIR-7831 retains strong RBD binding capability, although G339 is part of its epitope, the G339D mutation in Omicron does not appear to affect VIR-7831's binding; however, VIR-7831's IC50 is reduced to 181 ng/mL, and may be subject to further reduction against Omicron with R346K. DXP-604's binding affinity against Omicron RBD is largely reduced compared to wildtype RBD; nevertheless, it can still neutralize Omicron at an IC50 of 287 ng/mL, a nearly 30-fold reduction compared to wildtype (Fig. 4a). Additionally, several NABs in Group E and F have shown high potency against Omicron and broad pan-sarbecovirus neutralization ability, promising for NAB drug development (Fig. 4b). Many more NABs identified from vaccinated SARS-CoV-1 convalescents are waiting to be characterized.

The high-throughput yeast screening method provides a laboratory means for quickly examining the epitope of a certain NAB; however, the current throughput using FACS is limited and can not be used to evaluate a large NAB library. By virtue of MACS, we are able to increase the throughput by two orders of magnitude. In doing so, we were able to gain statistical confidence for the survival proportion of anti-RBD NABs in each epitope group against Omicron. The experimental accuracy for predicting the neutralization reduction for single amino acid mutations is relatively high (Extended Data Fig. 8a, b); however, current mutation screening through yeast display could not effectively probe the consequence of multiple mutations simultaneously, which requires further technical optimization.

To date, a large number of SARS-CoV-2 anti-RBD NABs have been identified from convalescents and vaccinees. The most potent NABs are frequently found in Groups A–D as we described above, which tend to directly interfere with the binding of ACE2. Nevertheless, the neutralizing powers of these NABs are often abrogated by RBD mutations in the evolutionary arms race between SARS-CoV-2 and human humoral immunity. Indeed, we showed that Omicron would escape the majority of SARS-CoV-2 NABs in this collection (Extended Data Fig. 5e). On the other hand, Groups E and F NABs are less affected by Omicron, likely because they are not abundant in population⁴⁸, hence exerting less evolutionary pressure for RBD to mutate in the corresponding epitope groups. These NABs target conserved RBD regions in sarbecovirus and therefore are ideal targets for future development of pan-sarbecovirus NAB drugs.

Online content

Any methods, additional references, Nature Research reporting summaries, source data, extended data, supplementary information,

acknowledgements, peer review information; details of author contributions and competing interests; and statements of data and code availability are available at <https://doi.org/10.1038/s41586-021-04385-3>.

1. Starr, T. N. et al. Prospective mapping of viral mutations that escape antibodies used to treat COVID-19. *Science* **371**, 850–854, <https://doi.org/10.1126/science.abf9302> (2021).
2. Starr, T. N., Greaney, A. J., Dingens, A. S. & Bloom, J. D. Complete map of SARS-CoV-2 RBD mutations that escape the monoclonal antibody LY-CoV555 and its cocktail with LY-CoV016. *Cell Rep Med* **2**, 100255, <https://doi.org/10.1016/j.xcrm.2021.100255> (2021).
3. Barnes, C. O. et al. SARS-CoV-2 neutralizing antibody structures inform therapeutic strategies. *Nature* **588**, 682–687, <https://doi.org/10.1038/s41586-020-2852-1> (2020).
4. Yuan, M. et al. Structural and functional ramifications of antigenic drift in recent SARS-CoV-2 variants. *Science* **373**, 818–823, <https://doi.org/10.1126/science.abb1139> (2021).
5. Dejnirattisai, W. et al. The antigenic anatomy of SARS-CoV-2 receptor binding domain. *Cell* **184**, 2183–2200 e2122, <https://doi.org/10.1016/j.cell.2021.02.032> (2021).
6. Pinto, D. et al. Cross-neutralization of SARS-CoV-2 by a human monoclonal SARS-CoV antibody. *Nature* **583**, 290–295, <https://doi.org/10.1038/s41586-020-2349-y> (2020).
7. Yuan, M. et al. A highly conserved cryptic epitope in the receptor binding domains of SARS-CoV-2 and SARS-CoV. *Science* **368**, 630–633, <https://doi.org/10.1126/science.abb7269> (2020).
8. Callaway, E. Heavily mutated Omicron variant puts scientists on alert. *Nature* **600**, 21, <https://doi.org/10.1038/d41586-021-03552-w> (2021).
9. Callaway, E. & Ledford, H. How bad is Omicron? What scientists know so far. *Nature*, <https://doi.org/10.1038/d41586-021-03614-z> (2021).
10. Li, Q. et al. SARS-CoV-2 501Y.V2 variants lack higher infectivity but do have immune escape. *Cell* **184**, 2362–2371 e2369, <https://doi.org/10.1016/j.cell.2021.02.042> (2021).
11. Cao, Y. et al. Humoral immune response to circulating SARS-CoV-2 variants elicited by inactivated and RBD-subunit vaccines. *Cell Res* **31**, 732–741, <https://doi.org/10.1038/s41422-021-00514-9> (2021).
12. Starr, T. N. et al. Deep Mutational Scanning of SARS-CoV-2 Receptor Binding Domain Reveals Constraints on Folding and ACE2 Binding. *Cell* **182**, 1295–1310 e1220, <https://doi.org/10.1016/j.cell.2020.08.012> (2020).
13. Gu, H. et al. Adaptation of SARS-CoV-2 in BALB/c mice for testing vaccine efficacy. *Science* **369**, 1603–1607, <https://doi.org/10.1126/science.abc4730> (2020).
14. Cerutti, G. et al. Potent SARS-CoV-2 neutralizing antibodies directed against spike N-terminal domain target a single supersite. *Cell Host Microbe* **29**, 819–833 e817, <https://doi.org/10.1016/j.chom.2021.03.005> (2021).
15. McCallum, M. et al. N-terminal domain antigenic mapping reveals a site of vulnerability for SARS-CoV-2. *Cell* **184**, 2332–2347 e2316, <https://doi.org/10.1016/j.cell.2021.03.028> (2021).
16. Greaney, A. J. et al. Complete Mapping of Mutations to the SARS-CoV-2 Spike Receptor-Binding Domain that Escape Antibody Recognition. *Cell Host Microbe* **29**, 44–57 e49, <https://doi.org/10.1016/j.chom.2020.11.007> (2021).
17. Cao, Y. et al. Potent Neutralizing Antibodies against SARS-CoV-2 Identified by High-Throughput Single-Cell Sequencing of Convalescent Patients' B Cells. *Cell* **182**, 73–84 e16, <https://doi.org/10.1016/j.cell.2020.05.025> (2020).
18. Ju, B. et al. Human neutralizing antibodies elicited by SARS-CoV-2 infection. *Nature* **584**, 115–119, <https://doi.org/10.1038/s41586-020-2380-z> (2020).
19. Shi, R. et al. A human neutralizing antibody targets the receptor-binding site of SARS-CoV-2. *Nature* **584**, 120–124, <https://doi.org/10.1038/s41586-020-2381-y> (2020).
20. Wu, Y. et al. A noncompeting pair of human neutralizing antibodies block COVID-19 virus binding to its receptor ACE2. *Science* **368**, 1274–1278, <https://doi.org/10.1126/science.abc2241> (2020).
21. Yuan, M. et al. Structural basis of a shared antibody response to SARS-CoV-2. *Science* **369**, 1119–1123, <https://doi.org/10.1126/science.abc2321> (2020).
22. Robbiani, D. F. et al. Convergent antibody responses to SARS-CoV-2 in convalescent individuals. *Nature* **584**, 437–442, <https://doi.org/10.1038/s41586-020-2456-9> (2020).
23. Liu, L. et al. Potent neutralizing antibodies against multiple epitopes on SARS-CoV-2 spike. *Nature* **584**, 450–456, <https://doi.org/10.1038/s41586-020-2571-7> (2020).
24. Baum, A. et al. Antibody cocktail to SARS-CoV-2 spike protein prevents rapid mutational escape seen with individual antibodies. *Science* **369**, 1014–1018, <https://doi.org/10.1126/science.abd0831> (2020).
25. Brouwer, P. J. M. et al. Potent neutralizing antibodies from COVID-19 patients define multiple targets of vulnerability. *Science* **369**, 643–650, <https://doi.org/10.1126/science.abc5902> (2020).
26. Rogers, T. F. et al. Isolation of potent SARS-CoV-2 neutralizing antibodies and protection from disease in a small animal model. *Science* **369**, 956–963, <https://doi.org/10.1126/science.abc7520> (2020).
27. Piccoli, L. et al. Mapping Neutralizing and Immunodominant Sites on the SARS-CoV-2 Spike Receptor-Binding Domain by Structure-Guided High-Resolution Serology. *Cell* **183**, 1024–1042 e1021, <https://doi.org/10.1016/j.cell.2020.09.037> (2020).
28. Zost, S. J. et al. Potently neutralizing and protective human antibodies against SARS-CoV-2. *Nature* **584**, 443–449, <https://doi.org/10.1038/s41586-020-2548-6> (2020).
29. Tortorici, M. A. et al. Ultrapotent human antibodies protect against SARS-CoV-2 challenge via multiple mechanisms. *Science* **370**, 950–957, <https://doi.org/10.1126/science.abe3354> (2020).
30. Lv, Z. et al. Structural basis for neutralization of SARS-CoV-2 and SARS-CoV by a potent therapeutic antibody. *Science* **369**, 1505–1509, <https://doi.org/10.1126/science.abc5881> (2020).
31. Zost, S. J. et al. Rapid isolation and profiling of a diverse panel of human monoclonal antibodies targeting the SARS-CoV-2 spike protein. *Nat Med* **26**, 1422–1427, <https://doi.org/10.1038/s41591-020-0998-x> (2020).
32. Seydoux, E. et al. Analysis of a SARS-CoV-2-Infected Individual Reveals Development of Potent Neutralizing Antibodies with Limited Somatic Mutation. *Immunity* **53**, 98–105 e105, <https://doi.org/10.1016/j.immuni.2020.06.001> (2020).

33. Kreye, J. et al. A Therapeutic Non-self-reactive SARS-CoV-2 Antibody Protects from Lung Pathology in a COVID-19 Hamster Model. *Cell* **183**, 1058-1069 e1019, <https://doi.org/10.1016/j.cell.2020.09.049> (2020).
34. Scheid, J. F. et al. B cell genomics behind cross-neutralization of SARS-CoV-2 variants and SARS-CoV. *Cell* **184**, 3205-3221 e3224, <https://doi.org/10.1016/j.cell.2021.04.032> (2021).
35. Tortorici, M. A. et al. Broad sarbecovirus neutralization by a human monoclonal antibody. *Nature* **597**, 103-108, <https://doi.org/10.1038/s41586-021-03817-4> (2021).
36. Dong, J. et al. Genetic and structural basis for SARS-CoV-2 variant neutralization by a two-antibody cocktail. *Nat Microbiol* **6**, 1233-1244, <https://doi.org/10.1038/s41564-021-00972-2> (2021).
37. Starr, T. N. et al. SARS-CoV-2 RBD antibodies that maximize breadth and resistance to escape. *Nature* **597**, 97-102, <https://doi.org/10.1038/s41586-021-03807-6> (2021).
38. Martinez, D. R. et al. A broadly cross-reactive antibody neutralizes and protects against sarbecovirus challenge in mice. *Sci Transl Med*, eabj7125, <https://doi.org/10.1126/scitranslmed.abj7125> (2021).
39. Onodera, T. et al. A SARS-CoV-2 antibody broadly neutralizes SARS-related coronaviruses and variants by coordinated recognition of a virus-vulnerable site. *Immunity* **54**, 2385-2398 e2310, <https://doi.org/10.1016/j.immuni.2021.08.025> (2021).
40. Raybould, M. I. J., Kovaltsuk, A., Marks, C. & Deane, C. M. CoV-AbDab: the coronavirus antibody database. *Bioinformatics* **37**, 734-735, <https://doi.org/10.1093/bioinformatics/btaa739> (2021).
41. Barnes, C. O. et al. Structures of Human Antibodies Bound to SARS-CoV-2 Spike Reveal Common Epitopes and Recurrent Features of Antibodies. *Cell* **182**, 828-842 e816, <https://doi.org/10.1016/j.cell.2020.06.025> (2020).
42. Hansen, J. et al. Studies in humanized mice and convalescent humans yield a SARS-CoV-2 antibody cocktail. *Science* **369**, 1010-1014, <https://doi.org/10.1126/science.abd0827> (2020).
43. Kim, S. I. et al. Stereotypic Neutralizing VH Clonotypes Against SARS-CoV-2 RBD in COVID-19 Patients and the Healthy Population. *bioRxiv*, 2020.2006.2026.174557, <https://doi.org/10.1101/2020.06.26.174557> (2020).
44. Du, S. et al. Structurally Resolved SARS-CoV-2 Antibody Shows High Efficacy in Severely Infected Hamsters and Provides a Potent Cocktail Pairing Strategy. *Cell* **183**, 1013-1023 e1013, <https://doi.org/10.1016/j.cell.2020.09.035> (2020).
45. Du, S. et al. Structures of SARS-CoV-2 B.1.351 neutralizing antibodies provide insights into cocktail design against concerning variants. *Cell Res* **31**, 1130-1133, <https://doi.org/10.1038/s41422-021-00555-0> (2021).
46. Harvey, W. T. et al. SARS-CoV-2 variants, spike mutations and immune escape. *Nat Rev Microbiol* **19**, 409-424, <https://doi.org/10.1038/s41579-021-00573-0> (2021).
47. Jones, B. E. et al. The neutralizing antibody, LY-CoV555, protects against SARS-CoV-2 infection in nonhuman primates. *Sci Transl Med* **13**, <https://doi.org/10.1126/scitranslmed.abf1906> (2021).
48. Tan, C. W. et al. Pan-Sarbecovirus Neutralizing Antibodies in BNT162b2-Immunized SARS-CoV-1 Survivors. *N Engl J Med* **385**, 1401-1406, <https://doi.org/10.1056/NEJMoa2108453> (2021).

Publisher's note Springer Nature remains neutral with regard to jurisdictional claims in published maps and institutional affiliations.

© The Author(s), under exclusive licence to Springer Nature Limited 2021

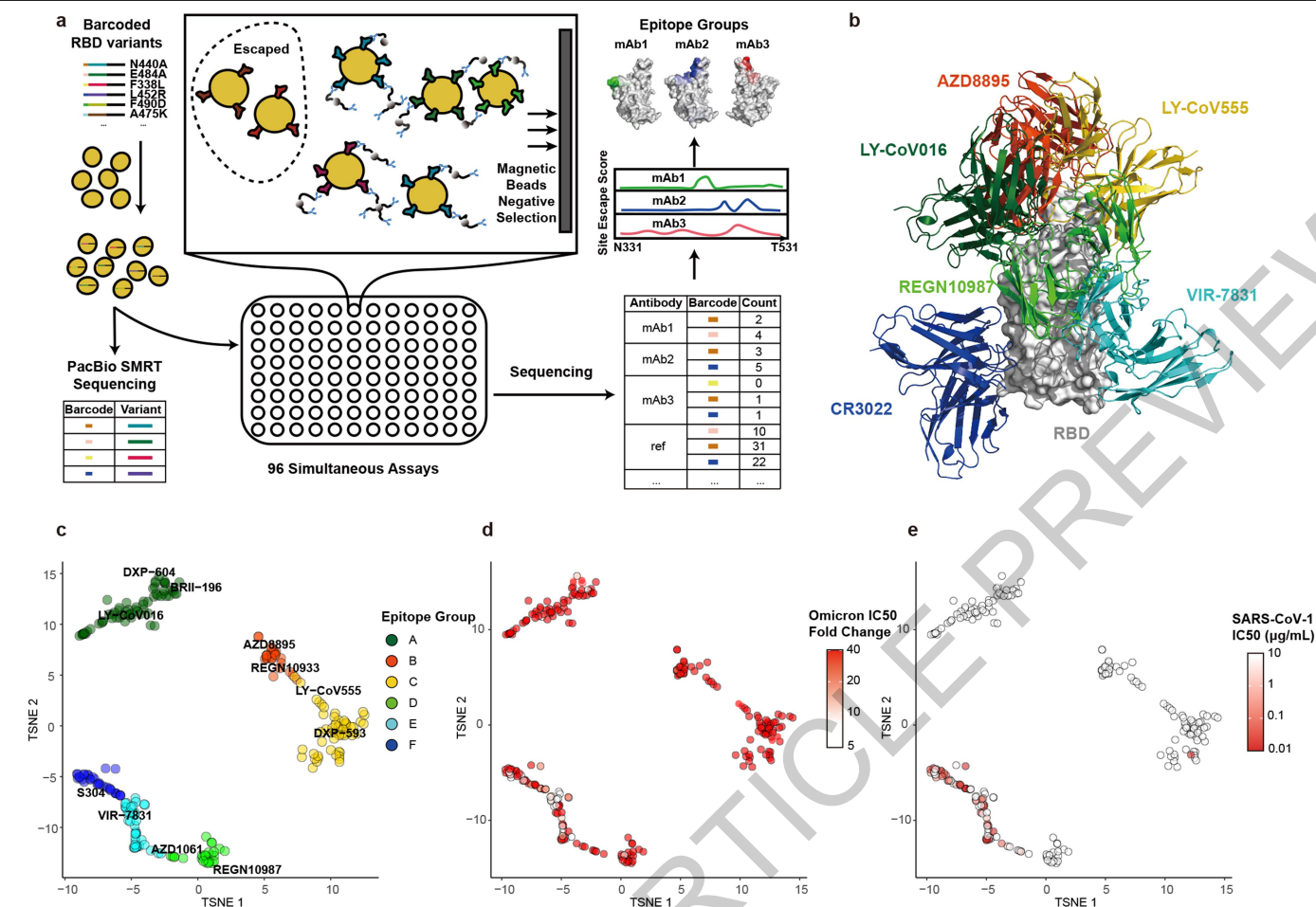


Fig. 1 | Omicron greatly reduces the neutralization potency of NAbs of diverse epitopes. a, Schematic of MACS-based high-throughput yeast display mutation screening. **b**, Representative NAb structures of each epitope group. **c**, t-SNE embedding and unsupervised clustering of SARS-CoV-2 human NAbs based on each antibody escaping mutation profile. A total of 6 epitope groups (Group A-F) could be defined. **d**, Neutralization of Omicron variant

(spike-pseudotyped VSV) by 247 RBD NAbs. Shades of red show IC50 fold change compared with D614G of each NAb. **e**, Neutralization of SARS-CoV-1 (spike-pseudotyped VSV) by 247 RBD NAbs. Shades of red show the IC50 value (μg/mL) of each NAb. All pseudovirus neutralization assays are conducted in biological duplicates or triplicates.

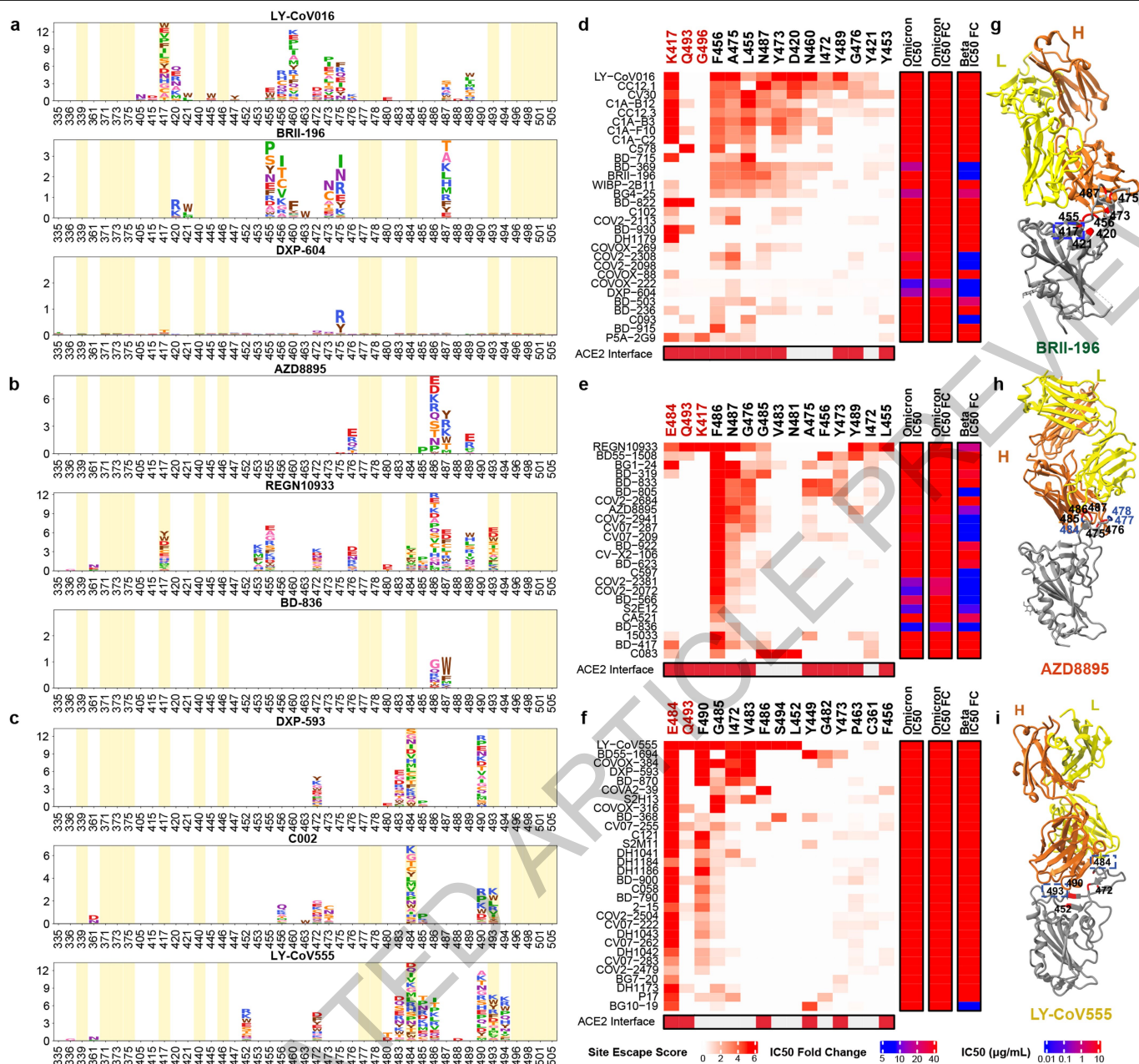


Fig. 2 | The neutralizing abilities of Group A-C NABs are mostly abolished by Omicron. a-c, Escaping mutation profiles of representative NABs for group A-C, respectively. For each site, the height of a letter indicates the detected mutation escape score of its corresponding residue. Sites mutated in Omicron are highlighted. **d-f,** Heatmaps of site escape scores for NABs of epitope group A-C, respectively. ACE2 interface residues are annotated with red blocks, and

mutated sites in Omicron are marked red. Annotations on the right side of heatmaps represent pseudovirus neutralizing IC₅₀ fold change (FC) for Omicron and Beta compared to D614G. **g-i,** Representative structures of group A-C antibodies in complex with RBD. Residues involved in important contacts are labeled. Omicron mutations are marked as blue. NAB escaping mutations (Omicron) inferred from yeast display are labeled with squares.

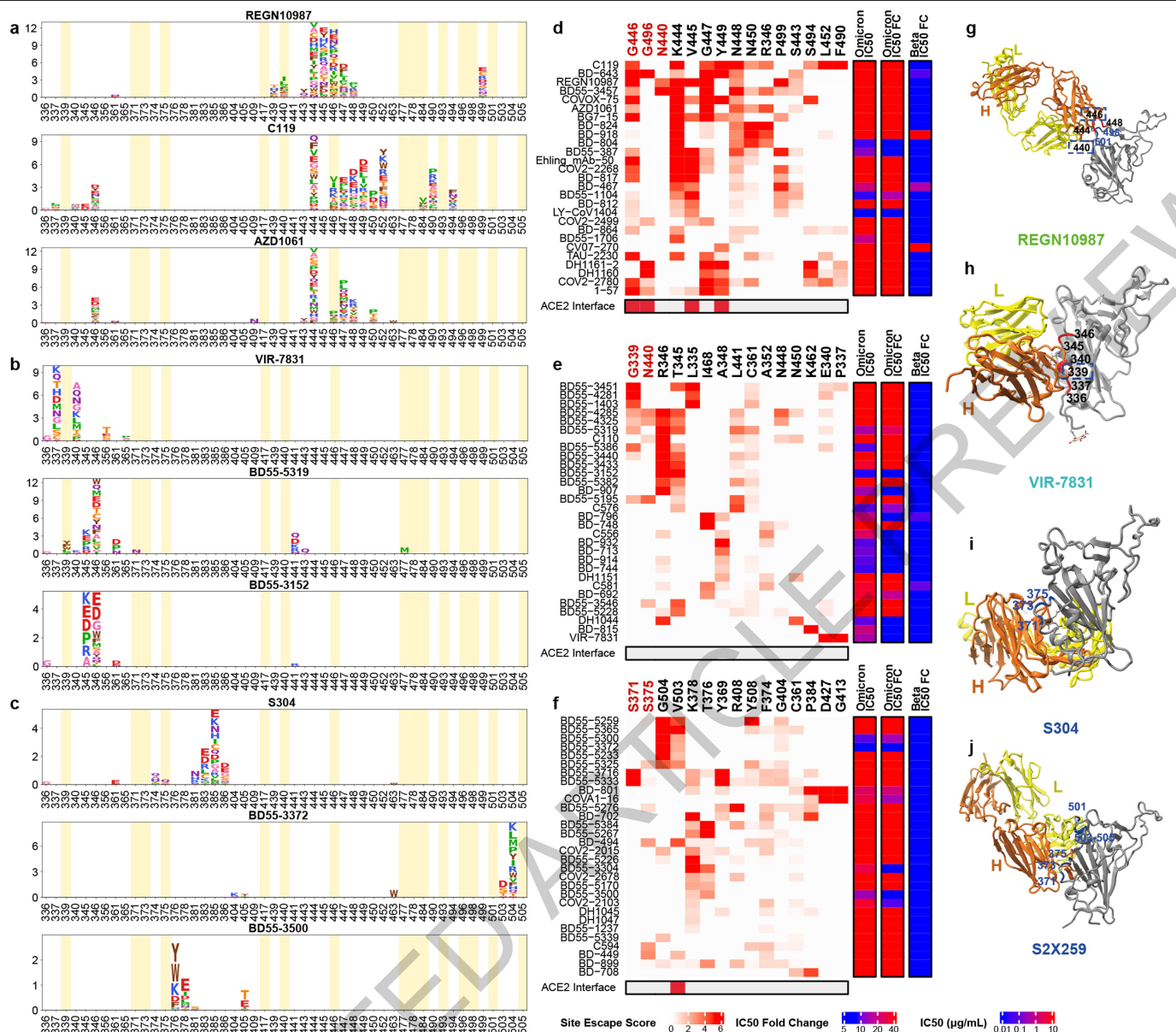


Fig. 3 | The majority of Group D-E NABs are escaped by Omicron.
a-c, Escaping mutation profiles of representative NABs for group D-E, respectively. For each site, the height of a letter indicates the detected mutation escape score of its corresponding residue. Sites mutated in Omicron are highlighted. **d-f**, Heatmaps of site escape scores for NABs of epitope group D-E, respectively. ACE2 interface residues are annotated with red blocks, and

mutated sites in Omicron are marked red. Annotations on the right side of heatmaps represent pseudovirus neutralizing IC50 fold change (FC) for Omicron and Beta compared to D614G. **g-j**, Representative structures of group D-E antibodies in complex with RBD. Residues involved in important contacts are labeled. Omicron mutations are marked as blue. NAB escaping mutations (Omicron) inferred from yeast display are labeled with squares.

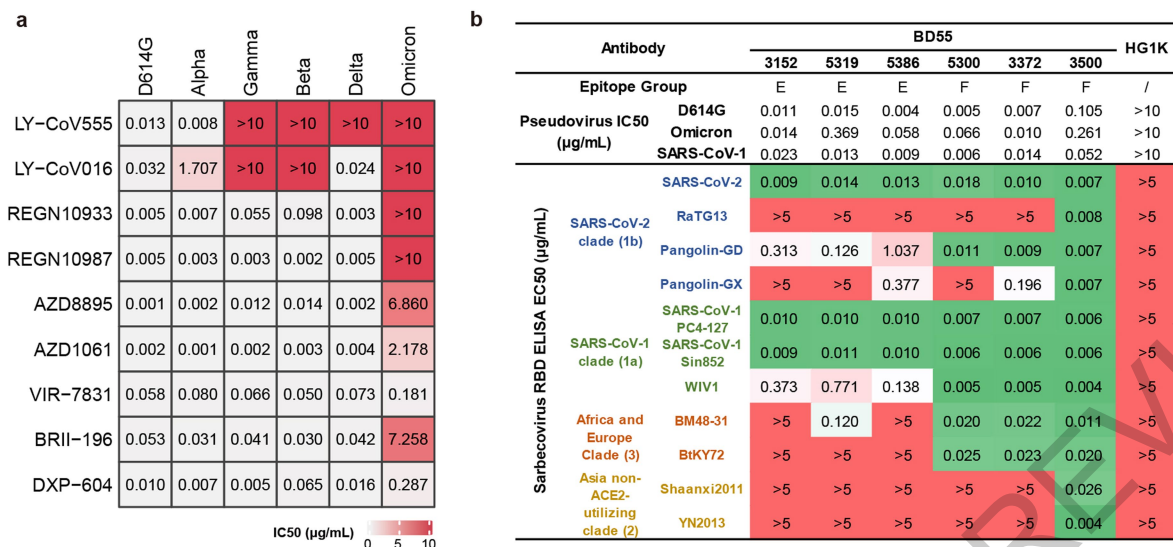


Fig. 4 | Omicron escapes most NAb drugs. a, Neutralization of SARS-CoV-2 variants of concern (pseudotyped VSV) by 9 NAb drugs. The pseudovirus neutralization assays for every VOC were performed in biological triplicates. IC50 labeled is the average of three replicates shown in Extended Data Fig. 9.

b, The sarbecovirus neutralization and binding capability of selected potent Omicron-neutralizing antibodies. Monoclonal antibody HG1K (IgG1 antibody against Influenza A virus subtype H7N9) was used as the negative control.

Methods

Human peripheral blood mononuclear cells isolation

SARS-CoV-2 convalescents, SARS-CoV-1 convalescents, and SARS-CoV-2 vaccinees were recruited on the basis of prior SARS-CoV-2 infection or SARS-CoV-1 infection or SARS-CoV-2 at Beijing Youan and Ditan hospital. Relevant experiments regarding SARS-CoV-2 convalescents and vaccinees were approved by the Beijing Youan Hospital Research Ethics Committee (Ethics committee archiving No. LL-2020-010-K). Relevant experiments regarding SARS-CoV-1 convalescents were approved by the Beijing Ditan Hospital Capital Medical University (Ethics committee archiving No. LL-2021-024-02). All participants provided written informed consent for the collection of information, and that their clinical samples were stored and used for research. Data generated from the research were agreed to be published. The detailed information of SARS-CoV-2 convalescents and vaccinees was previously described¹¹. Briefly, short-term convalescents' blood samples were obtained at day 62 on average after symptoms onset. Long-term convalescents' blood samples were obtained at day 371 on average after symptoms onset. No vaccination was received before blood collection. SARS-CoV-2 vaccinees' blood samples were obtained 2 weeks after complete vaccination of ZF2001 (RBD-subunit vaccine). For vaccinated SARS-CoV-1 convalescents (average age 58, $n = 21$), all recruited participants were previously identified for SARS-CoV-1 infection in 2003, and received two-dose vaccination of CoronaVac and a booster dose of ZF2001 with a 180-day-interval. 20 mL of blood samples of the vaccinated SARS-CoV-1 convalescents were obtained 2 weeks after the booster shot. Three Healthy vaccinated donor (average age 25) were also included to serve as negative control for FACS gating. Peripheral Blood Mononuclear Cells (PBMCs) were separated from whole blood samples based on the detailed protocol described previously¹¹. Briefly, blood samples were first diluted with 2% Fetal Bovine Serum (FBS) (Gibco) in Phosphate Buffer Saline (PBS) (Invitrogen) and subjected to Ficoll (Cytiva) gradient centrifugation. After red blood cell lysis and washing steps, PBMCs were resuspended with 2% FBS in PBS for downstream B cell isolation or 10% Dimethyl sulfoxide (Sigma-Aldrich) in FBS for further preservation.

Antigen-specific B cell sorting and sequencing

Starting with freshly isolated or thawed PBMCs, B cells were enriched by positive selection using a CD19+ B cell isolation kit according to the manufacturer's instructions (STEMCELL). The enriched B cells were stained in FACS buffer (1× PBS, 2% FBS, 1 mM EDTA) with the following anti-human antibodies and antigens: For every 10^6 cells, 3 μ L FITC anti-CD19 Antibody (Biolegend, 392508), 3 μ L FITC anti-CD20 Antibody (Biolegend, 302304), 3.5 μ L Brilliant Violet 421 anti-CD27 Antibody (Biolegend, 302824), 3 μ L PE/Cyanine7 anti-IgM (Biolegend, 314532), and fluorophore-labelled Receptor-Binding Domain (RBD) and ovalbumin (Ova) for 30 min on ice. Cells were stained with 5 μ L 7-AAD (eBioscience, 00-6993-50) for 10 minutes before sorting. Biotinylated receptor binding domain (RBD) of SARS (Sino biological, 40634-V27H-B) or SARS-CoV-2 (Sino biological, 40592-V27H-B) were multimerized with fluorescently labeled Streptavidin (SA) for 1 hour at 4 °C. RBD was mixed with SA-PE (Biolegend, 405204) and SA-APC (Biolegend, 405207) at a 4:1 molar ratio. For every 10^6 cells, 6 ng SA was used to stain. Single CD19 or CD20+, CD27+, IgM-, Ova-, RBD-PE+, RBD-APC+, live B cells were sorted on an Astrios EQ (Beckman Coulter) into PBS containing 30% FBS (Supplementary Data 2). FACS sorting were controlled by Summit 6.0 (Beckman Coulter). FACS data analyses were done by FlowJo 10.8. Cells obtained after FACS were sent for 5'-mRNA and V(D)J libraries preparation as previously described¹¹, which were further submitted to Illumina sequencing on a HiSeq 2500 platform, with the 26×91 pair-end reading mode.

V(D)J sequence data analysis

The raw FASTQ files were processed by Cell Ranger (version 6.1.1) pipeline using GRCh38 reference. Sequences were generated using

"cellranger multi" or "cellranger vdj" with default parameters. Antibody sequences were processed by IMG/DomainGapAlign (version 4.10.2) to obtain the annotations of V(D)J, regions of complementarity determining regions (CDR), and the mutation frequency^{49,50}. Mutation count divided by the length of the V gene peptide is defined as the amino acid mutation rate of the V gene.

Recombinant antibody production

Paired immunoglobulin heavy and light chain genes obtained from 10X Genomics V(D)J sequencing and analysis were submitted to recombinant monoclonal antibody synthesis. Briefly, heavy and light genes were cloned into expression vectors, respectively, based on Gibson assembly, and subsequently co-transfected into HEK293F cells (ThermoFisher, R79007). The secreted monoclonal antibodies from cultured cells were purified by protein A affinity chromatography. The specificities of these antibodies were determined by ELISA.

ELISA

ELISA plates were coated with RBD (SARS-CoV-2 WT, SARS-CoV-2 Omicron, SARS-CoV-1 RBD, Sino Biological Inc.) at 0.03 μ g/mL and 1 μ g/mL in PBS at 4 °C overnight. After standard washing and blocking, 100 μ L 1 μ g/mL antibodies were added to each well. After a 2 h incubation at room temperature, plates were washed and incubated with 0.08 μ g/mL goat anti-human IgG (H+L)/HRP (JACKSON, 109-035-003) for 1 h incubation at room temperature. Tetramethylbenzidine (TMB) (Solarbio) was then added, and the reaction was stopped by adding H₂SO₄. OD450 was measured by an ELISA microplate reader. An antibody is defined as ELISA-positive when the OD450 (1 μ g/mL RBD) is three times larger than the negative control, which utilizes an H7N9 specific human IgG1 antibody (HG1K, Sino Biology Cat #HG1K).

Pseudovirus neutralization assay

Pseudovirus neutralization assay was performed to evaluate neutralizing ability of antibodies. The detailed process was previously described by Cao et al.¹². Briefly, serially diluted antibodies were first incubated with pseudotyped virus for 1 h, and the mixture was then incubated with Huh-7 cells. After 24 h incubation in an incubator at 37 °C, cells were collected and lysed with luciferase substrate (PerkinElmer), then proceeded to luminescence intensity measurement by a microplate reader. IC50 was determined by a four-parameter non-linear regression model using PRISM (v9.0.1). Omicron pseudovirus contains the following mutations: A67V, H69del, V70del, T95I, G142D, V143del, Y144del, Y145del, N211del, L212I, ins214EPE, G339D, S371L, S373P, S375F, K417N, N440K, G446S, S477N, T478K, E484A, Q493R, G496S, Q498R, N501Y, Y505H, T547K, D614G, H655Y, N679K, P681H, N764K, D796Y, N856K, Q954H, N969K, L981F.

Biolayer interferometry

Biolayer interferometry assays were conducted on Octet® R8 Protein Analysis System (Fortebio) following the manufacturer's instruction. Briefly, after baseline calibration, Protein A biosensors (Fortebio) were immersed with antibodies to capture the antibody, then sensors were immersed in PBS with 0.05% Tween-20 to the baseline. After association with different concentrations of RBD of SARS-CoV-2 variants (Omicron RBD: 40592-V08H85), disassociation was conducted. Data were recorded using Octet BLI Discovery (12.2) and analyzed using Octet BLI Analysis (12.2).

RBD Deep Mutational Scanning Library construction

The yeast-display RBD mutant libraries used here were constructed as described by Starr et al.¹², based on the spike receptor-binding domain (RBD) from SARS-CoV-2 (NCBI GenBank: MN908947, residues N331-T531) with the modifications that instead of 16-nucleotide barcode (N16), a unique 26-nucleotide (N26), barcode was appended to each RBD variant as an identifier in order to decrease sequencing cost by

Article

eliminating the use of PhiX. Briefly, three rounds of mutagenesis PCR were performed with designed and synthesized mutagenetic primer pools; in order to solid our conclusion, we constructed two RBD mutant libraries independently. RBD mutant libraries were then cloned into pETcon 2649 vector and the assembled products were electroporated into electrocompetent DH10B cells to enlarge plasmid yield. Plasmid extracted from *E. coli* were transformed into the EBY100 strain of *Saccharomyces cerevisiae* via the method described by Gietz and Schiestl⁵¹. Transformed yeast population were screened on SD-CAA selective plate and further cultured in SD-CAA liquid medium at a large scale. The resulted yeast libraries were flash frozen by liquid nitrogen and preserved at -80°C.

PacBio library preparation, sequencing, and analysis

The correspondence of RBD gene sequence in mutant library and N26 barcode was obtained by PacBio sequencing. Firstly, the bacterially-extracted plasmid pools were digested by NotI restriction enzyme and purified by agarose gel electrophoresis, then proceed to SMRTbell ligation. Four RBD mutant libraries were sequenced in one SMRT cell on a PacBio Sequel II platform. PacBio SMRT sequencing subreads were converted to HiFi ccs reads with pbccs, and then processed with a slightly modified version of the script previously described¹² to generate the barcode-variant dictionary. To reduce noise, variants containing stop codons or supported by only one ccs read were removed from the dictionary and ignored during further analysis.

Magnetic-activated cell sorting (MACS)-based mutation escape profiling

ACE2 binding mutants were sorted based on magnetic beads to eliminate non-functional RBD variants. Briefly, the biotin binder beads (Thermo Fisher) were washed and prepared as the manufacturer's instruction and incubated with biotinylated ACE2 protein (Sino Biological Inc.) at room temperature with mild rotation. The ACE2 bound beads were washed twice and resuspend with 0.1% BSA buffer (PBS supplemented with 0.1% bovine serum albumin), and ready for ACE2 positive selection. Transformed yeast library were inoculated into SD-CAA and grown at 30°C with shaking for 16-18h, then back-diluted into SG-CAA at 23°C with shaking to induce RBD surface expression. Yeasts were collected and washed twice with 0.1% BSA buffer and incubated with aforementioned ACE2 bound beads at room temperature for 30min with mild rotating. Then, the bead-bound cells were washed, resuspend with SD-CAA media, and grown at 30°C with shaking. After overnight growth, the bead-unbound yeasts were separated with a magnet and cultured in a large scale. The above ACE2 positive selected yeast libraries were preserved at -80°C in aliquots as a seed bank for antibody escape mapping.

One aliquot of ACE2 positive selected RBD library was thawed and inoculated into SD-CAA, then grown at 30°C with shaking for 16-18h. 120 OD units were back-diluted into SG-CAA media and induced for RBD surface expression. Two rounds of sequential negative selection to sort yeast cells that escape Protein A conjugated antibody binding were performed according to the manufacturer's protocol. Briefly, Protein A magnetic beads (Thermo Fisher) were washed and resuspend in PBST (PBS with 0.02% Tween-20). Then beads were incubated with neutralizing antibody and rotated at room temperature for 30min. The antibody-conjugated beads were washed and resuspend in PBST. Induced yeast libraries were washed and incubated with antibody-conjugated beads for 30min at room temperature with agitation. The supernatant was separated and proceed to a second round of negative selection to ensure full depletion of antibody-binding yeast.

To eliminate yeast that did not express RBD, MYC-tag based RBD positive selection was conducted according to the manufacturer's protocol. First, anti-c-Myc magnetic beads (Thermo Fisher) were washed and resuspend with 1X TBST (TBS with Tween-20), then the

prepared beads were incubated for 30min with the antibody escaping yeasts after two rounds of negative selection. Yeasts bound by anti-c-Myc magnetic beads were wash with 1X TBST and grown overnight in SD-CAA to expand yeast population prior to plasmid extraction.

Overnight cultures of MACS sorted antibody-escaped and ACE2 pre-selected yeast populations were proceed to yeast plasmid extraction kit (Zymo Research). PCRs were performed to amplify the N26 barcode sequences as previously described¹³. The PCR products were purified with 0.9X Ampure XP beads (Beckman Coulter) and submitted to 75bp single-end Illumina Nextseq 500 sequencing.

Deep mutational scanning data processing

Raw single-end Illumina sequencing reads were trimmed and aligned to the reference barcode-variant dictionary generated as described above to get the count of each variant with *dms_variants* Python package (version 0.8.9). For libraries with N26 barcodes, we slightly modified the *illuminabarcodeparser* class of this package to tolerate one low sequencing quality base in the barcode region. The escape score of variant X is defined as $F \times (n_{X,ab} / N_{ab}) / (n_{X,ref} / N_{ref})$, where $n_{X,ab}$ and $n_{X,ref}$ is the number of detected barcodes for variant X, N_{ab} and N_{ref} are the total number of barcodes in antibody-selected (ab) library and reference (ref) library respectively as described by Starr et al¹². Different from FACS experiments, as we couldn't measure the number of cells retained after MACS selection precisely, here F is considered as a scaling factor to transform raw escape fraction ratios to 0-1 range, and is calculated from the first and 99th percentiles of raw escape fraction ratios. Scores less than the first percentile or larger than the 99th percentile are considered to be outliers and set to zero or one, respectively. For each experiment, barcodes detected by <6 reads in the reference library were removed to reduce the impact of sampling noise, and variants with ACE2 binding below -2.35 or RBD expression below -1 were removed as previously described¹². Finally, we built global epistasis models with *dms_variants* package for each library to estimate single mutation escape scores, utilizing the Python scripts provided by Greaney et al¹⁶. To reduce experiment noise, sites are retained for further analysis only if its total escape score is at least 0.01, and at least 3 times greater than the median score of all sites. For antibodies measured by 2 independent experiments, only sites which pass the filter in both experiments are retained. Logo plots in Fig. 2, Fig. 3, Extended Data Fig. 2 and Supplementary Data 1 are generated by Python package *logomaker* (version 0.8).

Antibody clustering

Antibody clustering and epitope group identification were performed based on the N×M escape score matrix, where N is the number of antibodies which pass the quality controlling filters, and M is the number of informative sites on SARS-CoV-2 RBD. Each entry of the matrix A_{nm} refers to the total escape score of all kinds of mutations on site m of antibody n. The dissimilarity between two antibodies is defined based on the Pearson's correlation coefficient of their escape score vectors, i.e. $D_{ij} = 1 - \text{Corr}(\mathbf{A}_i, \mathbf{A}_j)$, where $\text{Corr}(\mathbf{A}_i, \mathbf{A}_j) = \mathbf{x}_i \cdot \mathbf{x}_j / |\mathbf{x}_i| |\mathbf{x}_j|$ and vector $\mathbf{x}_i = \mathbf{A}_i - \text{Mean}(\mathbf{A}_i)$. Sites with at least 6 escaped antibodies (site escape score >1) were considered informative and selected for dimensionality reduction and clustering. We utilized R function *cmdscale* to convert the cleaned escape matrix into an N×6 feature matrix by multidimensional scaling (MDS) with the dissimilarity metric described above, followed by unsupervised k-medoids clustering within this 6-dimensional antibody feature space, using *pam* function of R package *cluster* (version 2.1.1). Finally, two-dimensional t-Distributed Stochastic Neighbor Embedding (tSNE) embeddings were generated with *Rtsne* package (version 0.15) for visualization. 2D t-SNE plots are generated by *ggplot2* (version 3.3.3), and heatmaps are generated by *ComplexHeatmap* package (version 2.6.2).

Reporting summary

Further information on research design is available in the Nature Research Reporting Summary linked to this paper.

Data availability

Processed escape maps for NABs are available in Supplementary Data 1 (as figures), or at <https://github.com/sunneyxielab/SARS-CoV-2-RBD-Abs-HTDMS> (as mutation escape score data). Raw Illumina and PacBio sequencing data are available on NCBI Sequence Read Archive BioProject PRJNA787091. We used vdj_GRCh38_alts_ensembl-5.0.0 as the reference of V(D)J alignment, which can be obtained from <https://support.10xgenomics.com/single-cell-vdj/software/downloads/latest>. IMGT/DomainGapAlign is based on the built-in latest IMGT antibody database, and we let the "Species" parameter as "Homo sapiens" while kept the others as default. FACS-based deep mutational scanning datasets could be downloaded from https://media.githubusercontent.com/media/jbloom-lab/SARS2_RBD_Ab_escape_maps/main/processed_data/escape_data.csv. Processed data of this study has been added to this repository as well.

Code availability

Scripts for analyzing SARS-CoV-2 escaping mutation profile data and for reproducing figures in this paper are available at <https://github.com/sunneyxielab/SARS-CoV-2-RBD-Abs-HTDMS>.

49. Ehrenmann, F., Kaas, Q. & Lefranc, M. P. IMGT/3Dstructure-DB and IMGT/DomainGapAlign: a database and a tool for immunoglobulins or antibodies, T cell receptors, MHC, IgSF and MhcSF. *Nucleic Acids Res* **38**, D301-307, <https://doi.org/10.1093/nar/gkp946> (2010).

50. Ehrenmann, F. & Lefranc, M. P. IMGT/DomainGapAlign: IMGT standardized analysis of amino acid sequences of variable, constant, and groove domains (IG, TR, MH, IgSF, MhSF). *Cold Spring Harb Protoc* **2011**, 737-749, <https://doi.org/10.1101/pdb.prot5636> (2011).
51. Gietz, R. D. & Schiestl, R. H. High-efficiency yeast transformation using the LiAc/SS carrier DNA/PEG method. *Nat Protoc* **2**, 31-34, <https://doi.org/10.1038/nprot.2007.13> (2007).

Acknowledgements We thank Professor Jesse Bloom for his generous gift of the yeast SARS-CoV-2 RBD libraries. We thank Beijing BerryGenomics for the help on DNA sequencing. We thank Sino Biological Inc. for the technical assistance on mAbs and Omicron RBD expression. We thank Sartorius (Shanghai) Trading Co., Ltd. for providing instrumental help with BLI measurement. We thank Jia Luo and Hongxia Lv (National Center for Protein Sciences and core facilities at School of Life Sciences at Peking University) for the help in flow cytometry. This project is financially supported by the Ministry of Science and Technology of China (CPL-1233).

Author contributions Y.C. and X.S.X. designed the study. Y.C. and F.S. coordinated the characterizations of the NABs. J.W., F.J., H.L., H.S. performed and analyzed the yeast display mutation screening experiments. T.X., W.J., X.Y., P.W., H.L. performed the pseudovirus neutralization assays. W.H., Q.L., T.L., Y.Y., Q.C., S.L., Y.W. prepared the VSV-based SARS-CoV-2 pseudovirus. A.Y., Y.W., S.Y., R.A., W.S. performed and analyzed the antigen-specific single B cell VDJ sequencing. X.N., R.A. performed the antibody BLI studies. Z.C., S.D., P.L., L.W., Z.Z., X.W., J.X. performed the antibody structural analyses. P.W., Y.W., J.W., H.S., H.L. performed the ELISA experiments. X.H. and R.J. coordinated the blood samples of vaccinated SARS-CoV-1 convalescents. Y.C., X.W., J.X., X.S.X. wrote the manuscript with inputs from all authors.

Competing interests X.S.X. and Y.C. are listed as inventors on a patent related to BD series antibodies and DXP-604 (PCT/CN2021/093305). X.S.X. and Y.C. are founders of Singlomics Biopharmaceuticals Inc. Other authors declare no competing interests.

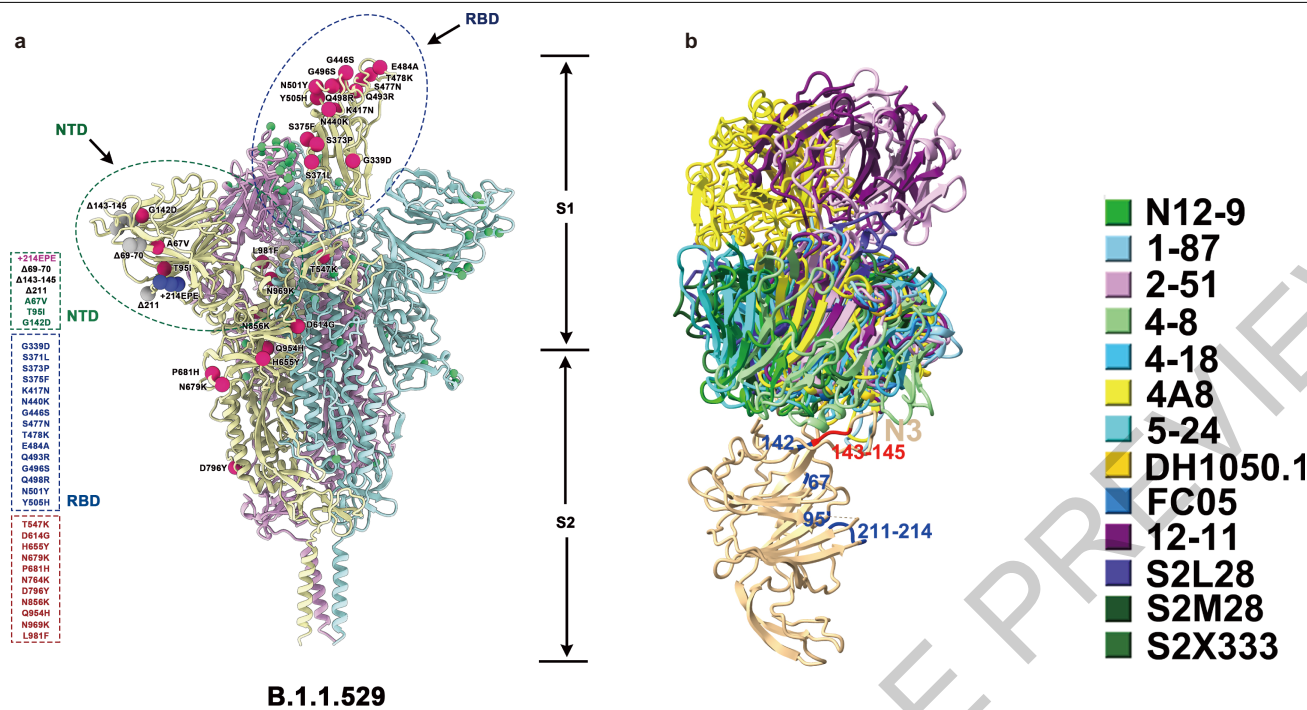
Additional information

Supplementary information The online version contains supplementary material available at <https://doi.org/10.1038/s41586-021-04385-3>.

Correspondence and requests for materials should be addressed to Yunlong Cao, Xiangxi Wang, Junyu Xiao, Yuchun Wang or Xiaoliang Sunney Xie.

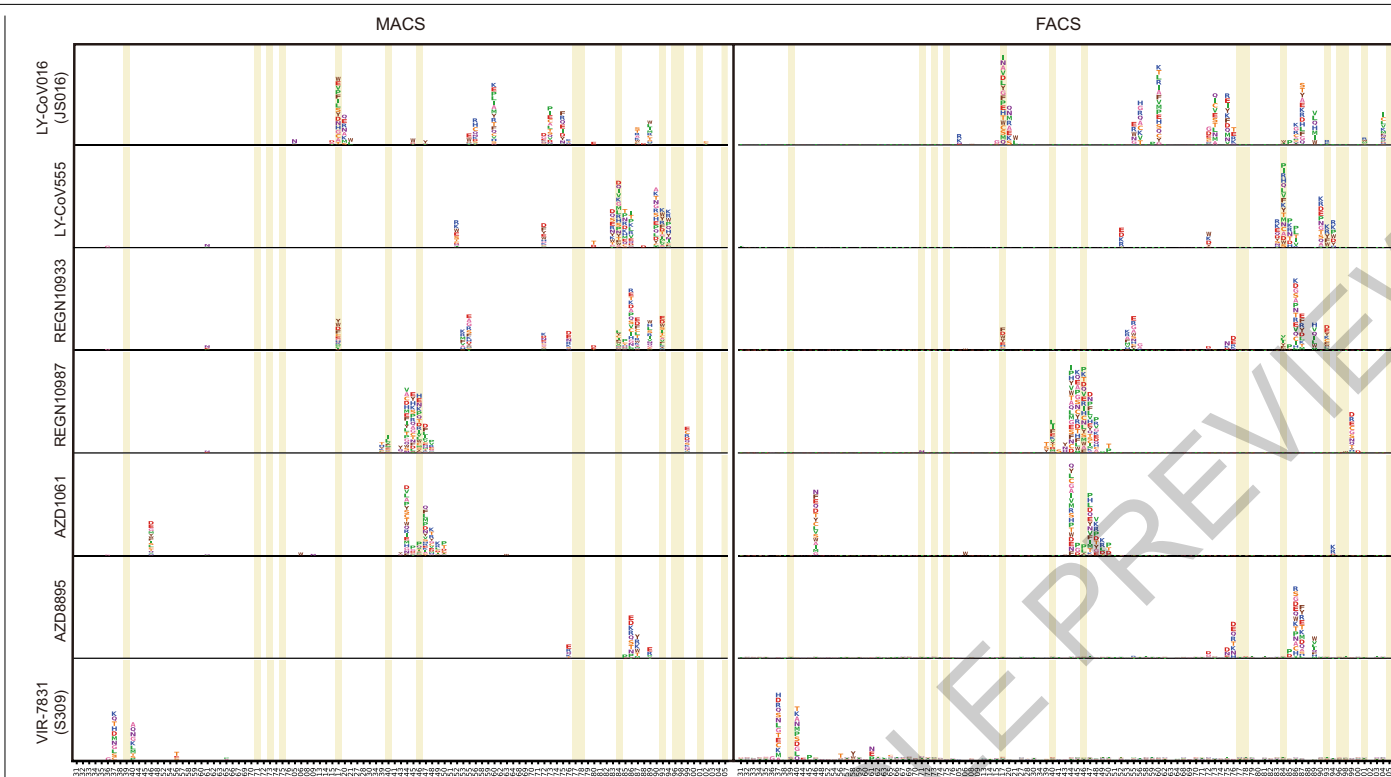
Peer review Peer review information *Nature* thanks the anonymous reviewer(s) for their contribution to the peer review of this work.

Reprints and permissions information is available at <http://www.nature.com/reprints>.



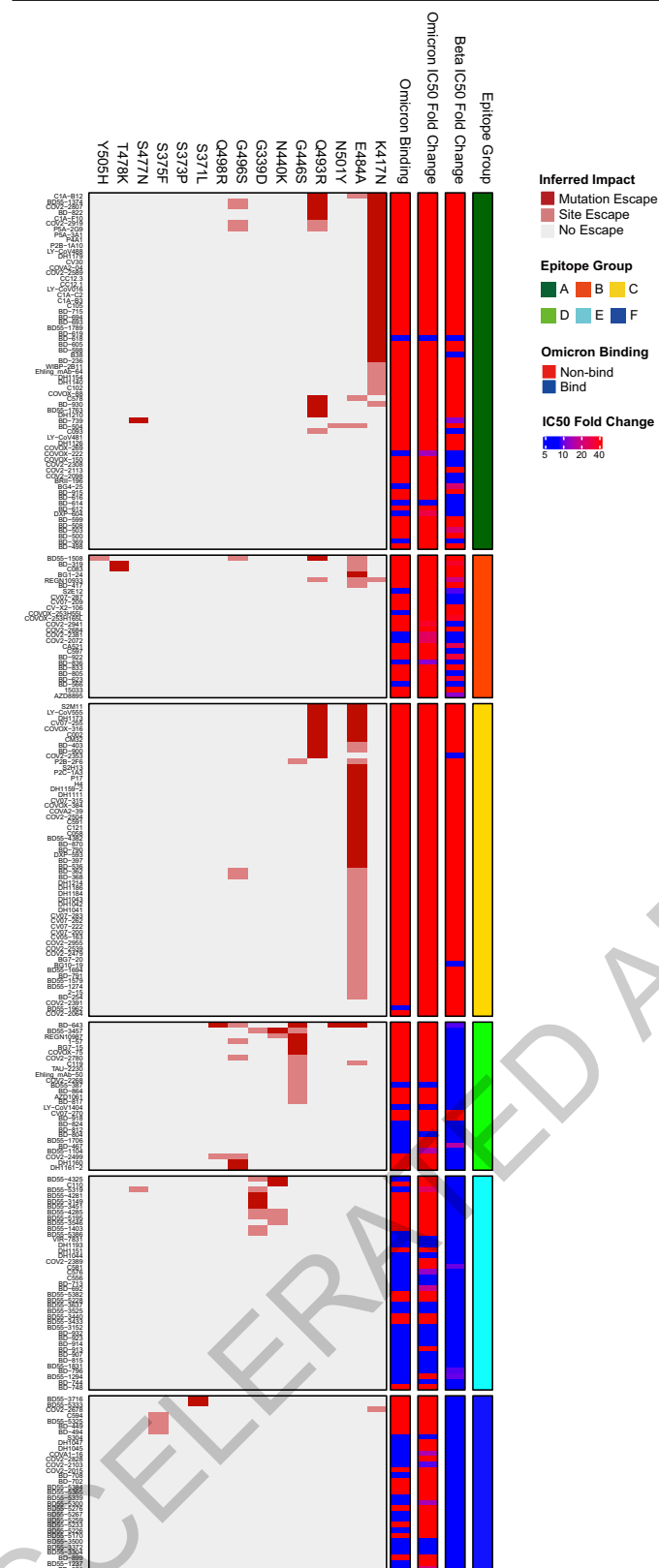
Extended Data Fig. 1 | Illustration of SARS-CoV-2 spike with Omicron's mutations. a, SARS-CoV-2 D614G spike protein structure overlaid with Omicron mutations. Omicron's (BA.1) popular mutations are marked by red

(for substitutions), blue (for insertions) and gray balls (for deletions). **b**, NTD-binding NABs shown together in complex with NTD. Substitutions and deletions of Omicron NTD are colored blue and red, respectively.

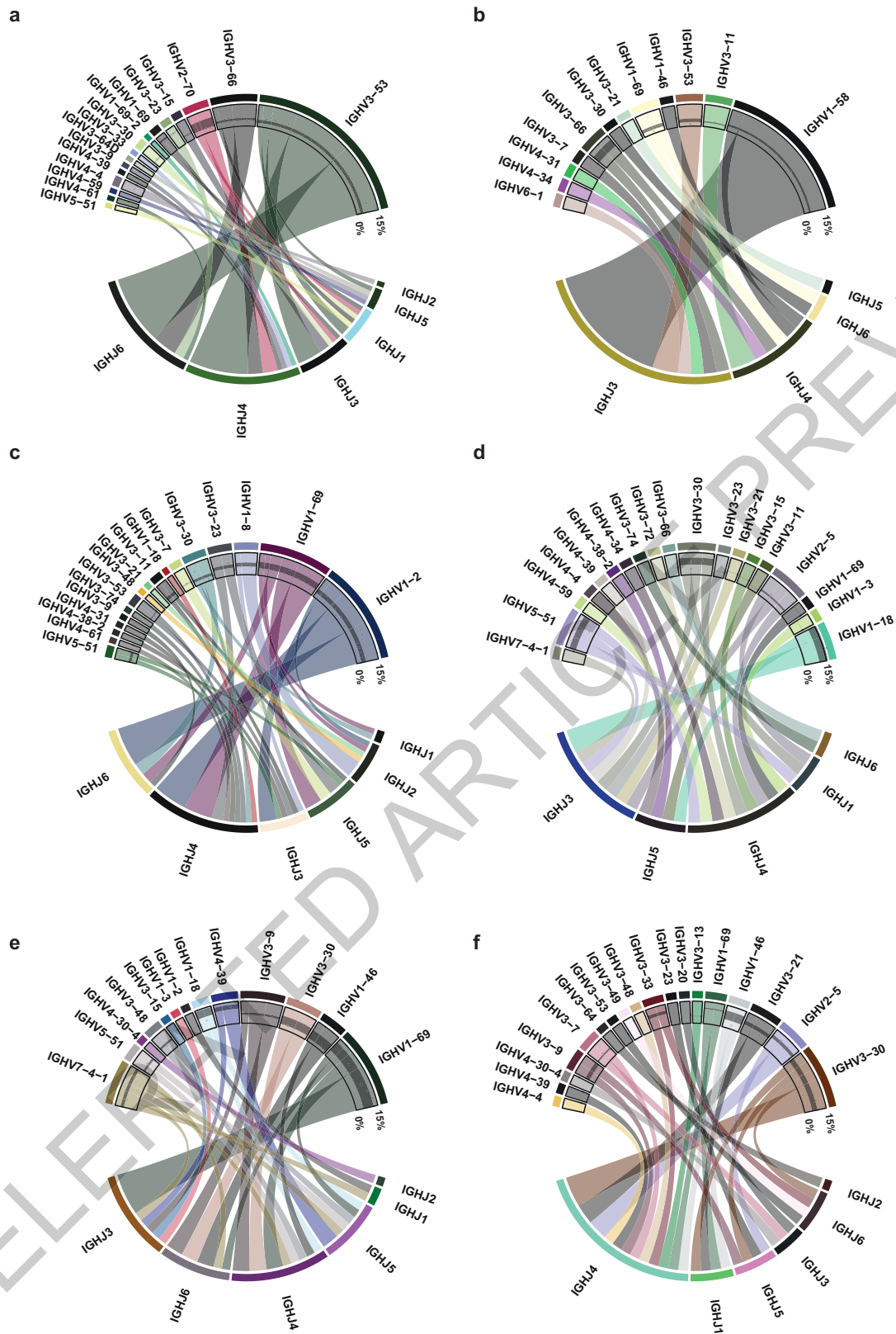


Extended Data Fig. 2 | Comparison between FACS and MACS-based deep mutational scanning. Deep mutational scanning maps with MACS-based (left) and FACS-based assays (right) of seven therapeutic neutralizing antibodies that have received emergency use authorization. Sites mutated in

the Omicron variant are highlighted. Mutation amino acids of each site are shown by single letters. The heights represent mutation escape score, and colors represent chemical properties. FACS-based data were obtained from public datasets by Jesse Bloom.

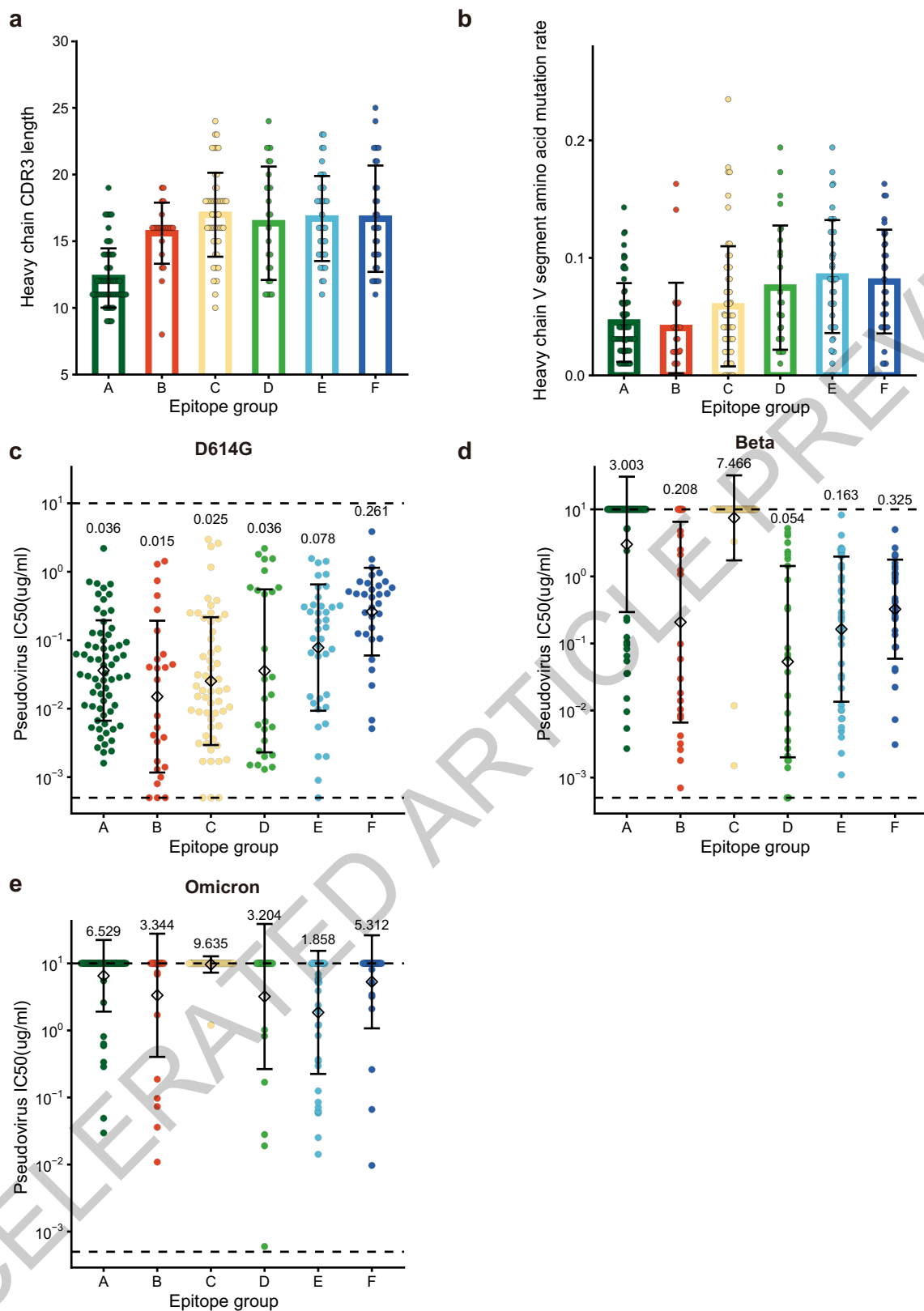


Extended Data Fig. 3 | Omicron neutralization IC50 fold-change distribution of 247 NABs of diverse epitopes. Fold-change of IC50 (VSV pseudovirus neutralization) compared to D614G by Beta and Omicron (BA.1) are shown for all 247 NABs tested. The impact of each RBD mutation of Omicron on NABs' binding is inferred from yeast display mutation screening. Each NAB's binding to Omicron RBD was validated through ELISA. All neutralization and ELISA assays were conducted in biological duplicates.



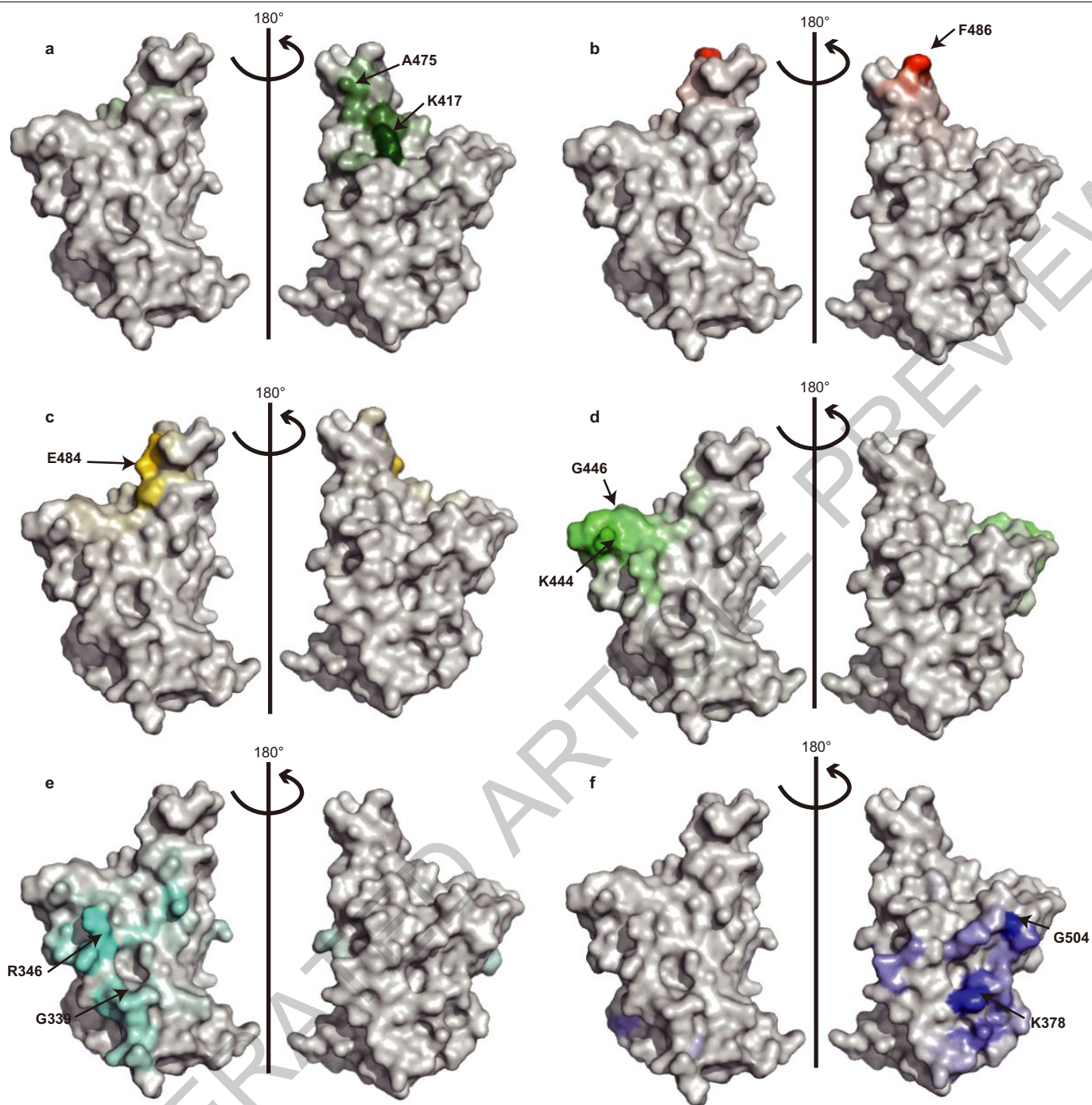
Extended Data Fig. 4 | Heavy chain V/J segment recombination of NAbs of each epitope group. a-f, Chord diagrams showing the heavy chain V segment and J segment recombination of epitope group A(a), B(b), C(c), D(d), E(e) and F(f). The width of the arc linking a V segment to a J segment indicates the

antibody number of the corresponding recombination. The inner layer scatter plots show the V segment amino acid mutation rate, while black strips show the 25%-75% quantile of mutation rates.



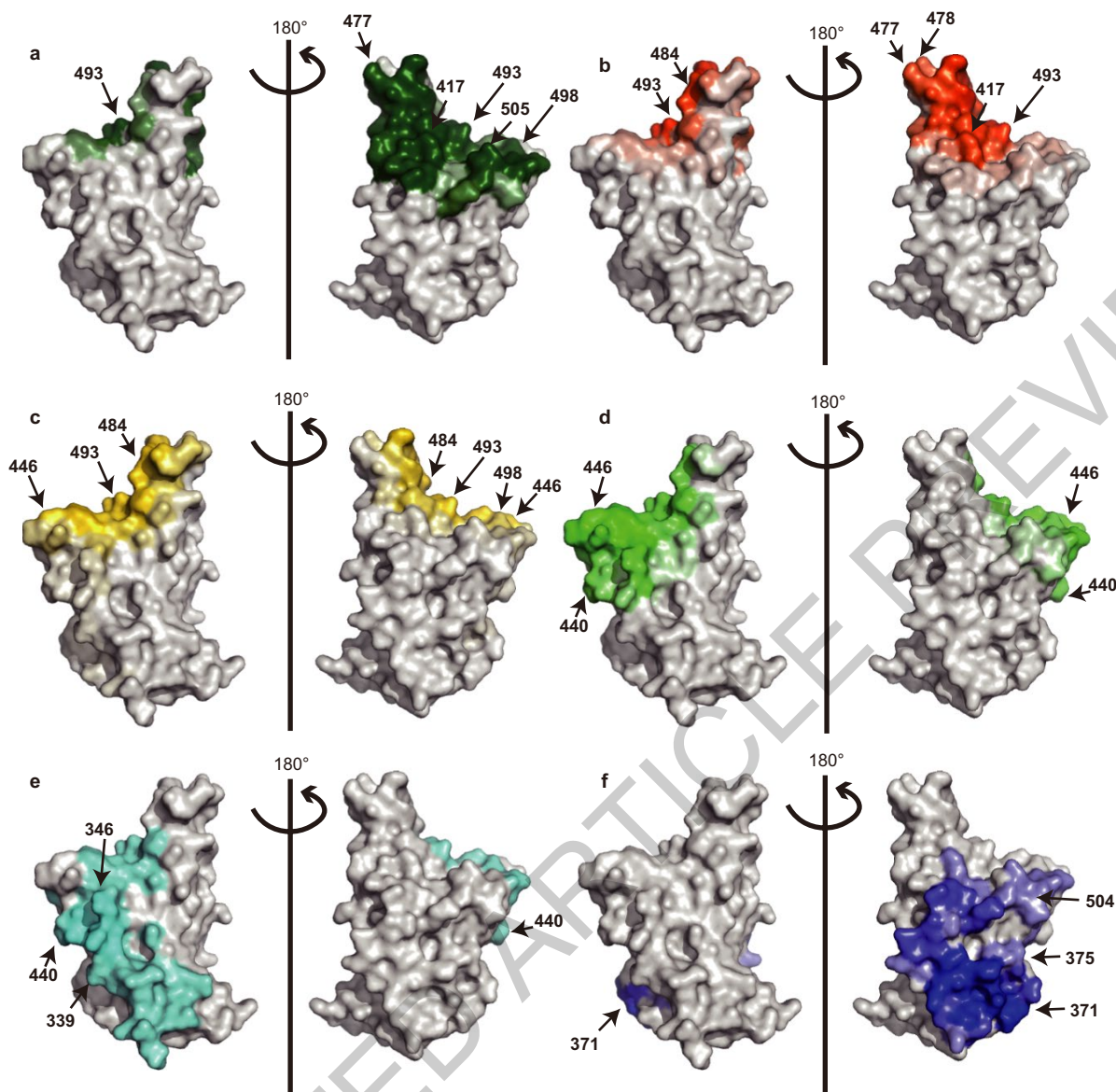
Extended Data Fig. 5 | Neutralization potency, heavy chain CDR3 length, and mutation rate distribution for NABs of each epitope group. **a**, The length of H chain complementarity-determining region 3 (HCDR3) amino acid sequence for NABs in each epitope group (n=66, 26, 57, 27, 39, 32 antibodies for epitope group A, B, C, D, E, F, respectively). HCDR3 lengths are displayed as mean \pm s.d. **b**, The V segment amino acid mutation rate for NABs in each epitope group (n=66, 26, 57, 27, 39, 32 antibodies for epitope group A, B, C, D, E, F,

respectively). Mutation rates are calculated and displayed as mean \pm s.d. **c-e**, The IC₅₀ against D614G(c), Beta(d), and Omicron(e) variants for NABs in each epitope group (n=66, 26, 57, 27, 39, 32 antibodies for epitope group A, B, C, D, E, F, respectively). IC₅₀ values are displayed as mean \pm s.d. in the log₁₀ scale. Pseudovirus assays for each variant are biologically replicated twice. Dotted lines show the detection limit, which is from 0.0005 μ g/mL to 10 μ g/mL. IC₅₀ geometric means are also labeled on the figure.



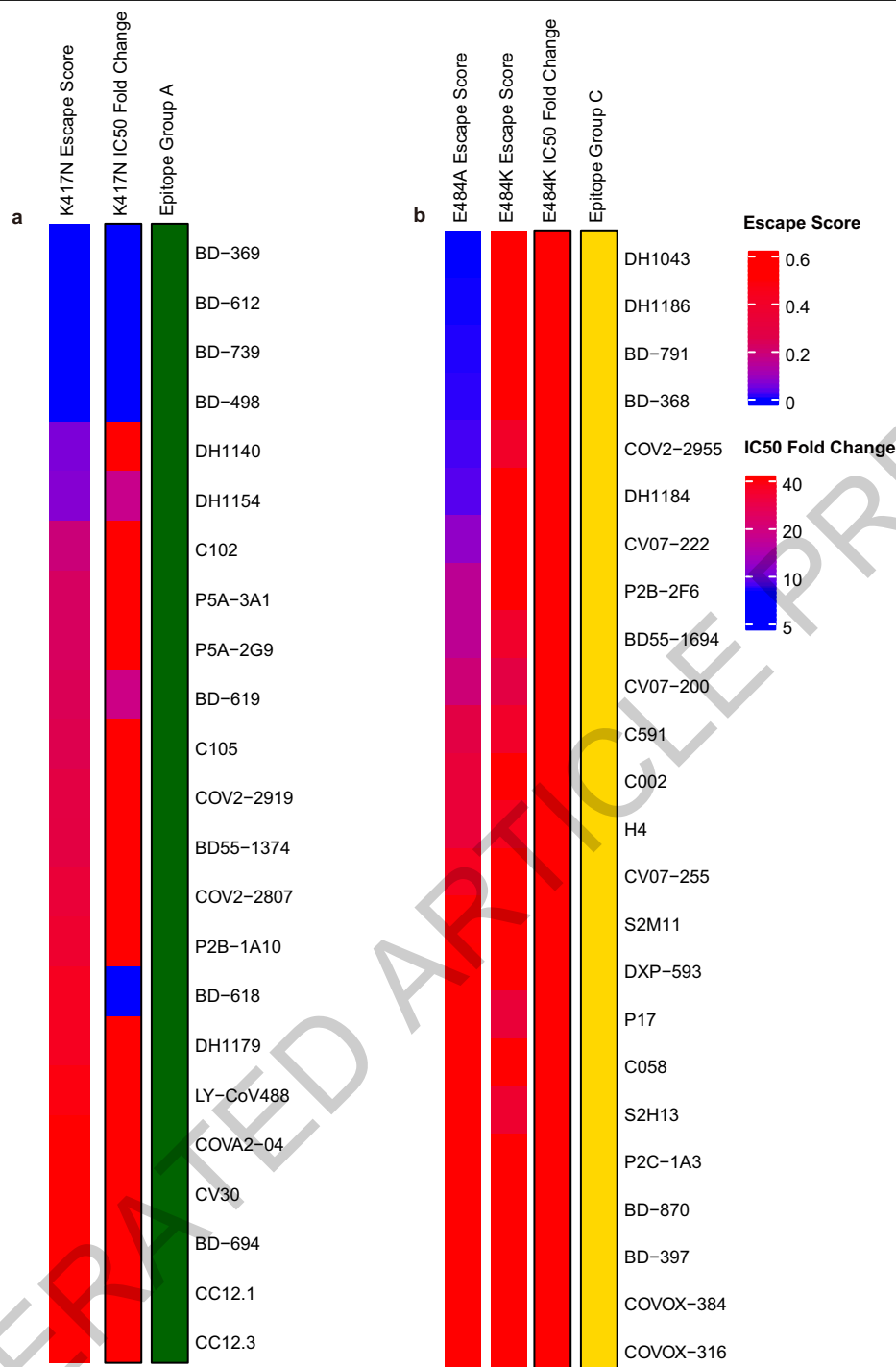
Extended Data Fig. 6 | Escape hotspots of different epitope groups on the RBD surface. a-f, Aggregated site escape scores of antibodies for epitope group A-F, respectively. Epitope groups are distinguished by distinct colors,

and the shades show normalized site escape scores. Escape hotspots of each epitope group are annotated by arrows.



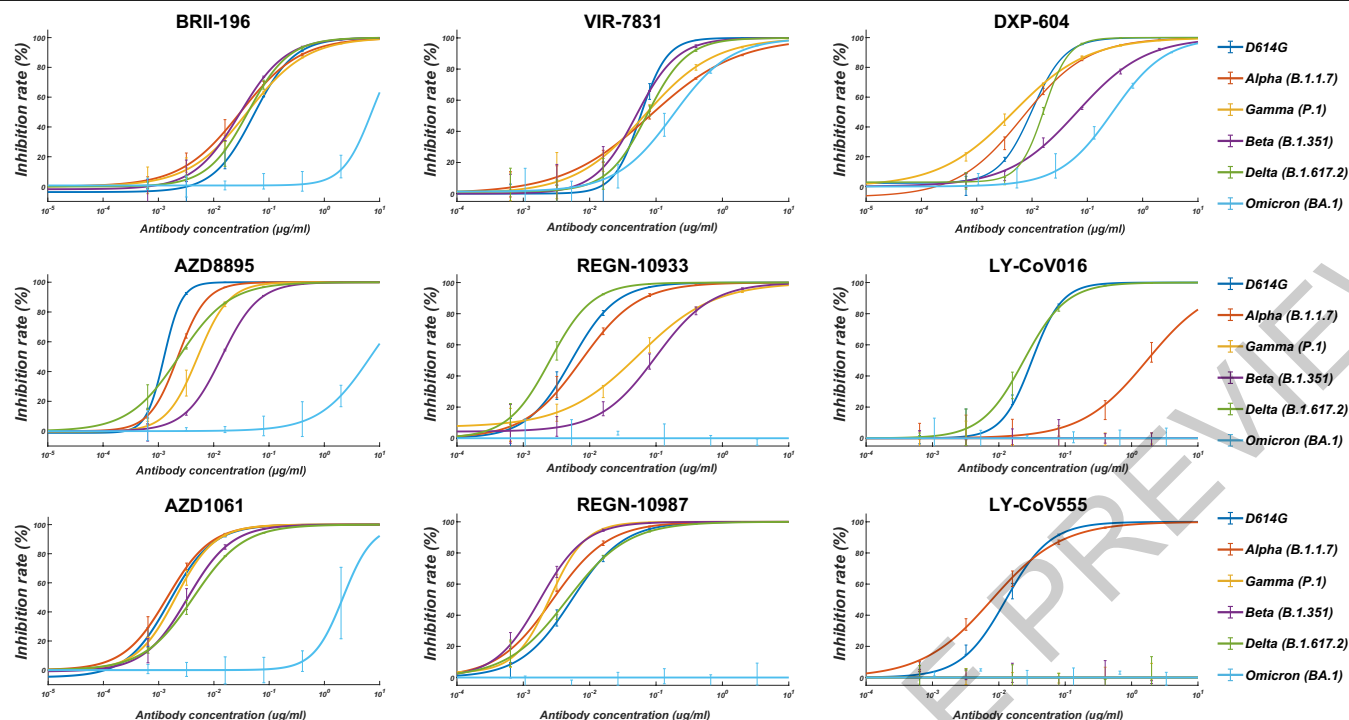
Extended Data Fig. 7 | Antibody-RBD interface distribution for NABs of each epitope group. a-f, Aggregated antibody-antigen interface of antibodies for epitope group A-F, respectively. Antibody-antigen interface was indicated from publicly available structures of neutralizing antibodies in complex with

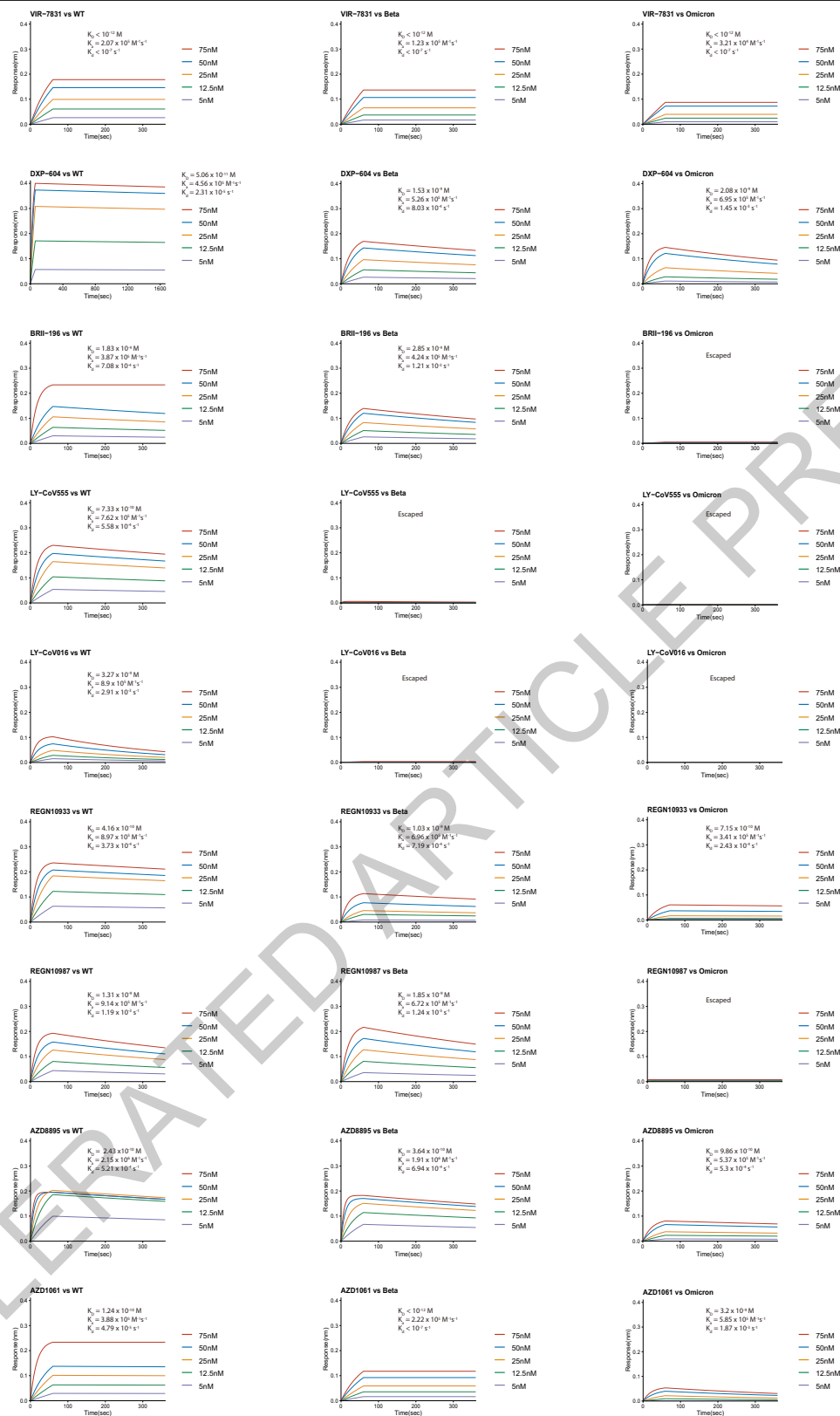
SARS-CoV-2 RBD. Different colors distinguish epitope groups, and the shade reflects group-specific site popularity to appear on the complex interface. Shared interface residues (Omicron) of each group are annotated.



Extended Data Fig. 8 | Comparison between mutation escape scores estimated from yeast display and neutralization of variants carrying corresponding mutations. a, K417N escape scores and corresponding K417N pseudovirus neutralizing IC50 fold change compared to D614G pseudovirus of

antibodies within epitope group A. **b,** E484K/E484A escape scores and corresponding E484K pseudovirus neutralizing IC50 fold change compared to D614G pseudovirus of antibodies within epitope group C.





Extended Data Fig. 10 | BLI response between NAb drugs and the RBD of SARS-CoV-2 wildtype, Beta, or Omicron strain. Antibodies were captured by Protein A sensor. The concentrations of RBD are shown in different colors.

Dissociation constant (K_D), association constant (k_a), and dissociation rate constant (k_d) are labeled. NABs without binding are marked as "Escaped".

Reporting Summary

Nature Portfolio wishes to improve the reproducibility of the work that we publish. This form provides structure for consistency and transparency in reporting. For further information on Nature Portfolio policies, see our [Editorial Policies](#) and the [Editorial Policy Checklist](#).

Statistics

For all statistical analyses, confirm that the following items are present in the figure legend, table legend, main text, or Methods section.

n/a Confirmed

- ☐ ☒ The exact sample size (n) for each experimental group/condition, given as a discrete number and unit of measurement
- ☐ ☒ A statement on whether measurements were taken from distinct samples or whether the same sample was measured repeatedly
- ☒ ☐ The statistical test(s) used AND whether they are one- or two-sided
Only common tests should be described solely by name; describe more complex techniques in the Methods section.
- ☒ ☐ A description of all covariates tested
- ☒ ☐ A description of any assumptions or corrections, such as tests of normality and adjustment for multiple comparisons
- ☐ ☒ A full description of the statistical parameters including central tendency (e.g. means) or other basic estimates (e.g. regression coefficient) AND variation (e.g. standard deviation) or associated estimates of uncertainty (e.g. confidence intervals)
- ☒ ☐ For null hypothesis testing, the test statistic (e.g. F , t , r) with confidence intervals, effect sizes, degrees of freedom and P value noted
Give P values as exact values whenever suitable.
- ☒ ☐ For Bayesian analysis, information on the choice of priors and Markov chain Monte Carlo settings
- ☒ ☐ For hierarchical and complex designs, identification of the appropriate level for tests and full reporting of outcomes
- ☐ ☒ Estimates of effect sizes (e.g. Cohen's d , Pearson's r), indicating how they were calculated

Our web collection on [statistics for biologists](#) contains articles on many of the points above.

Software and code

Policy information about [availability of computer code](#)

Data collection

BLI binding data collections were done by using Octet BLI Discovery 12.2.
FACS cell sorting were done by using Summit 6.0 (Beckman Coulter).

Data analysis

Neutralization assays were analyzed using PRISM (versions 9.0.1) as described in Methods.
BLI binding data analyses were done by using Octet BLI Analysis 12.2.
FACS data were analyzed by FlowJo 10.8.
V(D)J sequence data were analyzed using Cell Ranger (v6.1.1) and IMG/DomainGapAlign (v4.10.2).
Illumina barcodes sequencing data from deep mutational scanning experiments were analyzed using custom scripts (<https://github.com/sunneyxlab/SARS-CoV-2-RBD-Abs-HTDMS>) and package dms_variants (v0.8.9).
Logo plots were generated by Python package logomaker (version 0.8).
For unsupervised clustering, we utilized R function cmdscale to convert the cleaned escape matrix into an N×6 feature matrix by multidimensional scaling (MDS) with the dissimilarity metric, followed by unsupervised k-medoids clustering within this 6-dimensional antibody feature space, using pam function of R package cluster (version 2.1.1). Two-dimensional t-Distributed Stochastic Neighbor Embedding (tSNE) embeddings were generated with Rtsne package (version 0.15) for visualization. 2D t-SNE plots are generated by ggplot2 (version 3.3.3), and heatmaps are generated by ComplexHeatmap package (version 2.6.2).

For manuscripts utilizing custom algorithms or software that are central to the research but not yet described in published literature, software must be made available to editors and reviewers. We strongly encourage code deposition in a community repository (e.g. GitHub). See the Nature Portfolio [guidelines for submitting code & software](#) for further information.

Data

Policy information about [availability of data](#)

All manuscripts must include a [data availability statement](#). This statement should provide the following information, where applicable:

- Accession codes, unique identifiers, or web links for publicly available datasets
- A description of any restrictions on data availability
- For clinical datasets or third party data, please ensure that the statement adheres to our [policy](#)

Data availability Processed escape maps for NABs are available in Supplementary Data 1 (as figures), or at <https://github.com/sunneyxielab/SARS-CoV-2-RBD-Abs-HTDMS> (as mutation escape score data). Raw Illumina and PacBio sequencing data are available on NCBI Sequence Read Archive BioProject PRJNA787091. We used vdj_GRCh38_alts_ensembl-5.0.0 as the reference of V(D)J alignment, which can be obtained from <https://support.10xgenomics.com/single-cell-vdj/software/downloads/latest>. IMGT/DomainGapAlign is based on the built-in latest IMGT antibody database, and we let the "Species" parameter as "Homo sapiens" while kept the others as default. FACS-based deep mutational scanning datasets could be downloaded from https://media.githubusercontent.com/media/jbloomlab/SARS2_RBD_Ab_escape_maps/main/processed_data/escape_data.csv. Processed data of this study has been added to this repository as well.

Field-specific reporting

Please select the one below that is the best fit for your research. If you are not sure, read the appropriate sections before making your selection.

- ☒ Life sciences ☐ Behavioural & social sciences ☐ Ecological, evolutionary & environmental sciences

For a reference copy of the document with all sections, see nature.com/documents/nr-reporting-summary-flat.pdf

Life sciences study design

All studies must disclose on these points even when the disclosure is negative.

Sample size	A total of 247 neutralizing antibodies were characterized in the manuscript. No sample size calculation was performed. The sample size of this study is sufficient to obtain sufficient antibodies in each epitope group.
Data exclusions	A total of 271 NABs were initially planned for yeast-display , and 23 NABs failed due to technical errors and could not give any meaningful mutation data.
Replication	Experimental assays were performed in biological duplicate or triplicate according to or exceeding standards in the field. Specifically, we perform MACS-based mutation screening using two independently synthesized mutant libraries. We conducted all neutralization and ELISA assays in biological duplicates or triplicates. All replicates for neutralization and binding assays are successful.
Randomization	Randomization was not required since we were applying a uniform set of measurements across the panel of monoclonal antibodies
Blinding	Blinding was not required since we were applying a uniform set of measurements across the panel of monoclonal antibodies

Reporting for specific materials, systems and methods

We require information from authors about some types of materials, experimental systems and methods used in many studies. Here, indicate whether each material, system or method listed is relevant to your study. If you are not sure if a list item applies to your research, read the appropriate section before selecting a response.

Materials & experimental systems

n/a	Involved in the study
<input type="checkbox"/>	<input checked="" type="checkbox"/> Antibodies
<input type="checkbox"/>	<input checked="" type="checkbox"/> Eukaryotic cell lines
<input checked="" type="checkbox"/>	<input type="checkbox"/> Palaeontology and archaeology
<input checked="" type="checkbox"/>	<input type="checkbox"/> Animals and other organisms
<input type="checkbox"/>	<input checked="" type="checkbox"/> Human research participants
<input checked="" type="checkbox"/>	<input type="checkbox"/> Clinical data
<input checked="" type="checkbox"/>	<input type="checkbox"/> Dual use research of concern

Methods

n/a	Involved in the study
<input checked="" type="checkbox"/>	<input type="checkbox"/> ChIP-seq
<input type="checkbox"/>	<input checked="" type="checkbox"/> Flow cytometry
<input checked="" type="checkbox"/>	<input type="checkbox"/> MRI-based neuroimaging

Antibodies

Antibodies used

ELISA antibody detection: 109-035-003, Peroxidase-AffiniPure Goat Anti-Human IgG (H+L) , Jackson
 Negative control H7N9 human IgG1 antibody: HG1K, Sino Biology Cat #HG1K
 The enriched B cells were stained with the following anti-human antibodies and antigens: For every 10⁶ cells, 3 µL FITC anti-CD19 Antibody (Biolegend, 392508), 3 µL FITC anti-CD20 Antibody (Biolegend, 302304), 3.5 µL Brilliant Violet 421 anti-CD27 Antibody

(Biolegend, 302824), 3 μ L PE/Cyanine7 anti-IgM (Biolegend, 314532), and fluorophore-labelled Receptor-Binding Domain (RBD) and ovalbumin (Ova) for 30 min on ice. Cells were stained with 5 μ L 7-AAD (eBioscience, 00-6993-50) for 10 minutes before sorting. All neutralizing antibodies were expressed using HEK293F cell lines with codon-optimized cDNA and human IgG1 constant regions in house. The detailed sequence could be found in Supplementary Table 1 column I and J.

Validation

In this manuscript, we tested 247 anti-RBD SARS-CoV-2 human neutralizing IgG1 antibodies. All neutralizing antibodies were expressed using HEK293F cell lines with codon-optimized cDNA and human IgG1 constant regions. All neutralizing antibodies' species and specificity to RBD were validated by ELISA using goat anti-human IgG (H+L)/HRP. All antibodies neutralization ability was verified by VSV-based pseudovirus assays. Details and sequences for all SARS-CoV-2 neutralizing antibodies evaluated in this study is included in Supplementary Table 1. Reactivity and specificity of the primary antibodies listed above is based on the information on manufacturer's homepages.

Eukaryotic cell lines

Policy information about [cell lines](#)

Cell line source(s)

HEK293F for antibody production was received from ThermoFisher (R79007)
EBY100 (Yeast) was received from ATCC (ATCCMYA-4941);
Huh-7 for pseudovirus assays was received from Japanese Collection of Research Bioresources (JCRB 0403);

Authentication

No authentication was performed beyond manufacturer standards;

Mycoplasma contamination

Not tested for mycoplasma contamination;

Commonly misidentified lines (See [ICLAC](#) register)

No commonly misidentified cell lines were used in the study.

Human research participants

Policy information about [studies involving human research participants](#)

Population characteristics

The detailed information of SARS-CoV-2 convalescents and vaccinees was previously described in Cao et al., Cell Research, 2021, doi:10.1038/s41422-021-00514-9. Briefly, short-term convalescents' blood samples were obtained at day 62 on average after symptoms onset. Long-term convalescents' blood samples were obtained at day 371 on average after symptoms onset. No vaccination was received before blood collection. SARS-CoV-2 vaccinees' blood samples were obtained 2 weeks after complete vaccination of ZF2001 (RBD-subunit vaccine). For vaccinated SARS-CoV-1 convalescents (average age 58, n = 21), all recruited participants were identified for SARS-CoV-1 infection in 2003, and received two-dose vaccination of CoronaVac and a booster dose of ZF2001 with a 180-day-interval. Blood samples of vaccinated SARS-CoV-1 convalescents were obtained 2 weeks after the booster shot. Three Healthy vaccinated donor (average age 25) were also included to serve as negative control for FACS gating.

Recruitment

Patients were recruited on the basis of prior SARS-CoV-2 infection or SARS-CoV-1 infection or SARS-CoV-2 vaccination. The only exclusion criteria used were HIV or other debilitating diseases.

Ethics oversight

Relevant experiments regarding SARS-CoV-2 convalescents and vaccinees were approved by the Beijing Youan Hospital Research Ethics Committee (Ethics committee archiving No. LL-2020-010-K). Relevant experiments regarding SARS-CoV-1 convalescents were approved by the Beijing Ditan Hospital Capital Medical University (Ethics committee archiving No. LL-2021-024-02). Written informed consent was obtained from each participant in accordance with the Declaration of Helsinki. All participants provided written informed consent for the collection of information, and that their clinical samples were stored and used for research. Data generated from the research were agreed to be published.

Note that full information on the approval of the study protocol must also be provided in the manuscript.

Flow Cytometry

Plots

Confirm that:

- ☒ The axis labels state the marker and fluorochrome used (e.g. CD4-FITC).
- ☒ The axis scales are clearly visible. Include numbers along axes only for bottom left plot of group (a 'group' is an analysis of identical markers).
- ☒ All plots are contour plots with outliers or pseudocolor plots.
- ☒ A numerical value for number of cells or percentage (with statistics) is provided.

Methodology

Sample preparation

Whole blood samples from SARS-CoV-2 convalescents or vaccinees were mixed and subjected to Ficoll (Cytiva, 17-1440-03) gradient centrifugation after 1:1 dilution in PBS+2% FBS. After centrifugation, plasma was collected from upper layer and cells were harvested at the interface, respectively. PBMCs were further prepared through centrifugation, red blood cells lysis (Invitrogen™ eBioscience™ 1X RBC Lysis Buffer, 00-4333-57) and washing steps. Samples were stored in FBS (Gibco) with 10% DMSO (Sigma) in liquid nitrogen if not used for downstream process immediately. Cryopreserved PBMCs were thawed in DPBS+2% FBS (Stemcell, 07905). On the day of sorting, B cells were enriched using CD19+ B cell isolation kit according to the manufacturer's instructions (STEMCELL, 19054). Biotinylated receptor binding domain (RBD) of SARS (Sino biological, 40634-V27H-B) or SARS-CoV-2 (Sino biological, 40592-V27H-B) were multimerized with fluorescently labeled Streptavidin (SA) for 1 hour at 4°C. RBD was mixed with SA-PE (Biolegend, 405204) and SA-APC (Biolegend, 405207) at a 4:1 molar ratio. For every 10⁶ cells, 6 ng SA was used to stain.

Instrument

Astrios EQ (BeckMan Coulter)

Software

Summit 6.0 (Beckman Coulter) for cell sorting; FlowJo 10.8 for data analysis.

Cell population abundance

Memory B cell purity post-sorting is over 90% as measured by 10x sequencing.

Gating strategy

Single CD19 or CD20+, CD27+, IgM-, Ova-, RBD-PE+, RBD-APC+, live B cells were sorted on an Astrios EQ (BeckMan Coulter) into PBS containing 30% FBS. The detailed FSC/SSC gating scheme is showed in Supplementary Data 2. Gates are drawn to define positive cells on the basis of unvaccinated healthy donor control.

☒ Tick this box to confirm that a figure exemplifying the gating strategy is provided in the Supplementary Information.